AN ABSTRACT OF THE THESIS OF

Arthur Darrell Stump for the Doctor of Philosophy Degree
(Name) (Degree)

in Inorganic Chemistry
(Major)

Date thesis is presented June 25, 1963

Title The Microstructure of Marine Sediments

Abstract approved [redacted]
(Major professor)

The surface areas and pore size distributions of a series of terrigenous marine sediments were measured by gas adsorption. The sediment samples were taken from the continental terrace off the coast of Oregon near Newport. Sampling stations ranged up to 35 miles off shore between 44°20' and 45° north latitude. Surface areas were calculated from linear B.E.T. plots made from nitrogen and water vapor adsorption isotherms. Pore size distributions were calculated from the nitrogen desorption isotherms using the method developed by Pierce. The Frenkel-Halsey-Hill equation was used to calculate the number of statistical layers in the correction value for multilayer adsorption. Low angle x-ray diffraction was used to identify the clay mineral content of the region. Surface areas, porosity, and x-ray diffractograms were correlated with average grain size, percent ferromagnetic material, depth and distance from shore. A simple rapid method for determining surface areas of terrigenous marine sediment was developed. The pore size distribution calculations were programmed for a computer.

THE MICROSTRUCTURE OF MARINE SEDIMENTS

by

ARTHUR DARRELL STUMP

A THESIS

submitted to

OREGON STATE UNIVERSITY

in partial fulfillment of
the requirements for the
degree of

DOCTOR OF PHILOSOPHY

September 1963

APPROVED:

[redacted]

Professor of Chemistry

In Charge of Major

[redacted]

Head of Department of Chemistry

[redacted]

Dean of Graduate School

Date thesis is presented June 25, 1963

Typed by Penny A. Self

ACKNOWLEDGEMENTS

The author wishes to thank Dr. Wayne V. Burt and the Oceanography Department for financial assistance in this project. The project would have been impossible without the aid of this department and the R/V "Acona" as well as the marine geologists of the Oceanography Department who collected the sediment samples.

Gratitude must be expressed to the Mathematics Department for the use of their computer. Further thanks must be expressed to Gary Ford for his aid in programming the calculations.

Thanks go also to the soils department and, especially to Dr. M.E. Harwood, for aiding with the x-ray diffraction work and for the use of their x-ray diffraction apparatus.

The author also wishes to express his appreciation to Dr. W.H. Slabaugh for his guidance, understanding and patience during the whole project as well as for the use of his laboratory.

TABLE OF CONTENTS

TABLE OF CONTENTS Continued

LIST OF FIGURES

LIST OF FIGURES Continued

LIST OF TABLES

THE MICROSTRUCTURE OF MARINE SEDIMENTS

INTRODUCTION

Purpose

The investigation herein described has a twofold purpose: (1) to define the structure of the particles in marine sediments and (2) to develop and refine the techniques of surface measurements by gas adsorption for adaptation to marine sediments.

The surface areas and pore volume and size distributions of micropores within the particles were measured by gas adsorption techniques. The structure and expansion properties of the clay minerals in the marine sediments were investigated by x-ray diffraction.

An improved and rapid method of gas adsorption surface area measurement was developed for terrigenous marine sediments. The calculation of pore size distributions was refined and adapted for computer calculation.

It is expected that the information concerning the microstructure of marine sediments will further the understanding of chemical reactions taking place at the liquid solid interface at the bottom of the sea and further the knowledge of the sorption of both organic and inorganic materials upon marine sediments.

Classification of Marine Sediments

A marine sediment is any solid material that has been deposited in an environment of saline water. The sediment can (1) precipitate directly from solution (hydrogenic), (2) be formed and transported by living organisms (biogenic), (3) originate from land erosion (lithogenic), (4) enter the sea from the atmosphere and settle to the bottom (atmogenic), or (5) be of extraterrestrial origin (astrogenic).

No marine sediment is one pure mineral. It is always a mixture which varies widely from place to place. The two types of minerals that compose the major part of marine sediments are: (1) the carbonates (mainly calcium), which are mostly biogenic, consisting of skeletal remains of zooplankton (some carbonates are also hydrogenic precipitates);(2) siliceous material, which can be both biogenic remains of siliceous skeletons of planktonic plants and animals, and lithogenic deposits of clay minerals, metal oxides and the various forms of silica. Sediments are sometimes classified mineralogically with respect to the variation in composition of these two materials as (14, p. 110-146):

1. Calcareous: sediments containing 5 to 60 percent magnesium and calcium carbonate.

2. Argillaceous: sediments that yield by chemical analysis from 52 to 58 percent SiO_2 and are low in carbonates.

3. Siliceous: when chemical analysis produces over 58 percent SiO_2.

The more general classification of marine sediments according to type is the following (43, p. 972-992):

1. Pelagic: are deposits in deep water far from shore and may be predominately either organic or inorganic in origin. They are usually light colored, reddish-brown and fine grained.

2. Terrigenous: occur near shore, usually on the continental shelf and slope, and contain coarse material of lithogenic origin.

3. Neritic: is a narrow region between pelagic and terrigenous consisting of a mixture of terrigenous and pelagic material (12, p. 112-119). The neritic zone is a boundary region and for the purpose of this investigation will be considered as part of the terrigenous zone.

Pelagic deposits are subclassified according to their mode of deposition as:

1. Inorganic deposits: those that contain less than

30 percent organic remains, called red clay.

2. Organic deposits: those which contain more than 30 percent material of biogenic origin. These organic deposits are known as oozes and are classified into subdivisions according to the type of material and the organism forming them as:

a. Calcareous oozes: those containing more than 30 percent $CaCO_3$ representing skeletal remains of various plants and animals. Calcareous oozes are subdivided into classes according to the organism predominating in the sediment as:

1. Globigerina ooze: where the $CaCO_3$ is chiefly composed of the tests of pelagic foraminifera.
2. Pteropod ooze: consists of conspicuous shells of pelagic mollusks.
3. Coccolith ooze: named for the large number of coccoliths and rhobdoliths that form the protective structures of minute coccolithophoridae.

b. Siliceous oozes: Pelagic deposits which contain large percentages of siliceous material produced by planktonic plants and animals. There are two subdivisions based on the predominance of the forms present as:

1. Diatom ooze: containing large amounts of diatom

frustules, therefore produced by planktonic plants.

2. Radiolarian ooze: because of the large amount of skeletal remains of the planktonic animal radiolarian.

Terrigenous sediments cannot be classified into types as easily as pelagic sediments because the former do not occur in as large regions of similar environment as the latter. Terrigenous sediments cover a much smaller area of the sea floor than pelagic. They also vary much more over a smaller distance. Their change in composition is quite drastic in very short distances from the shore. Terrigenous sediments have varying composition from coast to coast and in different locations on one coast line. These variations reflect the differences in the composition of the land area from which the materials come as well as variations in the marine environment of the particular coastal area. The three most important marine factors affecting terrigenous sediments are (1) the turbulence of the water, (2) the dissolved oxygen content and (3) biological activity.

One of the better systems for naming terrigenous sediments is the descriptive trinomial nomenclature. Color, texture, and the name of the principal mineral are used to make up the descriptive names of the sediments.

Marine sediments can be varying shades of white, yellow, blue, red, black or mixtures of these colors. Shelf sediments are usually dark in color ranging from green or brown to blue depending on the local environment.

The texture is defined as follows:

1. Sand: more than 80 percent of the particles having a diameter greater than 62μ.

2. Silty sand: Between 50 and 80 percent of the particles coarser than 62μ.

3. Sandy silt: more than 50 percent coarser than 5μ and more than 20 percent coarser than 62μ.

4. Silty mud: more than 50 percent coarser than 5μ and less than 20 percent coarser than 62μ.

5. Clayey mud: less than 50 percent coarser than 5μ.

The mode of transport or deposition such as "glacial" may be included in the name, if it is important.

For example, following the trinomial nomenclature a sediment near the Oregon coast in the vicinity of Newport may be classed as gray montmorillonitic silty mud and one further from the coast as green glauconitic sand.

The Clay Minerals

The word clay plays a dual role in describing sediments. It is the term applied to particles with diameters less then 4μ but also to a specific class of minerals. In order to avoid confusion the word "clay" will be used for particle size and "clay mineral" will designate the class of minerals. To further understand the structure of terrigenous marine sediments it is helpful to look briefly at the basic structural units encountered in these minerals. The primary arrangement of the silicon ion, as predicted by electrostatic valence, is the tetrahedral structure, shown in Figure 1 as the orthosilicate unit. The four covalent bonds are distributed tetrahedrally. These four bonds are of equal strength and the arrangement is symmetrical. The silica tetrahedra can combine in many ways, extending themselves in one, two or three dimensions. They can also form a variety of ring structures. No matter how complicated the network, the complex will be basically combinations of the silica tetrahedra. The grouping that is important to building a clay mineral is the layer unit $(Si_2O_5)^=$, a unit capable of extending itself continuously in two dimensions.

The other structural unit of layered clay minerals is the alumina octahedron. The arrangement of six groups around an aluminum ion is also shown in Figure 1. $Al_2(OH)_6$ in the form of gibbsite, Figure 1, is also a laminar type crystal

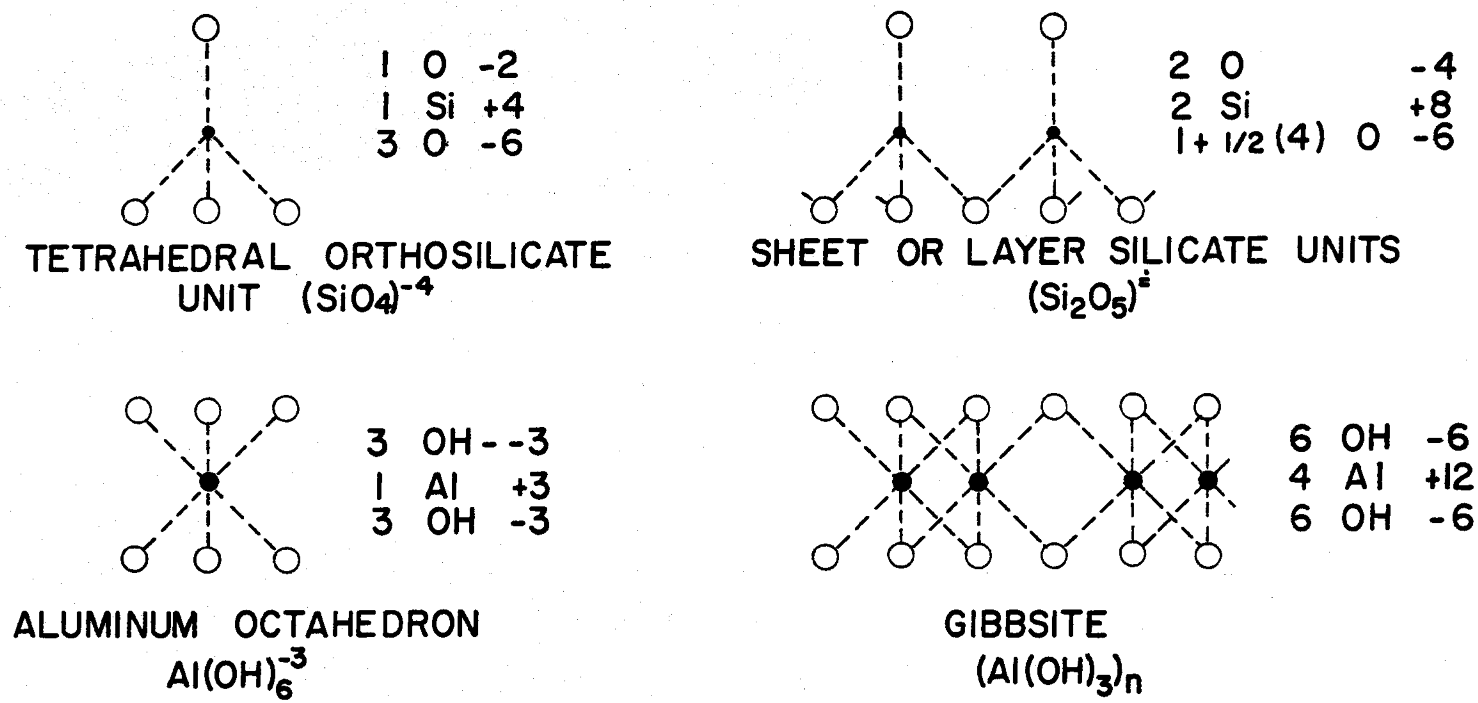

FIGURE 1

Layered Clay Minerals

The building blocks of layered clay minerals. All atoms have been projected into one plane.

capable of extending itself continuously in two dimensions.

If we visualize the two negative charges of the $(Si_2O_5)^=$ unit as satisfied by two hydrogen ions in $H_2Si_2O_5$ and imagine a condensation reaction between gibbsite and $H_2Si_2O_5$ as:

(1) $2\,H_2Si_2O_5 + Al_4(OH)_{12} \longrightarrow Al_4Si_4O_{10}(OH)_8 + 4\,H_2O$

where both groups can extend in two dimensions, the result would be the 1-1 clay mineral kaolinite shown in Figure 2.

Another situation where two $H_2Si_2O_5$ units condense on each side of the gibbsite unit:

(2) $4\,H_2Si_2O_5 + Al_4(OH)_{12} \longrightarrow Al_4Si_8O_{20}(OH)_4 + 8\,H_2O$

produces the mineral pyrophyllite, Figure 2, that Pauling first described (35, p. 123-129). His description helped to explain the structure of clay minerals.

When clay mineral crystals aggregate, the plates stack up like a deck of playing cards. The crystal platelets of kaolin are bound very tightly because of the hydrogen bonds formed between the oxygen atoms on one side and the OH^- groups on the other. Large amounts of energy are required to separate the platelets. Pyrophyllite, on the other hand, has no $(OH)^-$

FIGURE 2

(a) Pyrophyllite structure

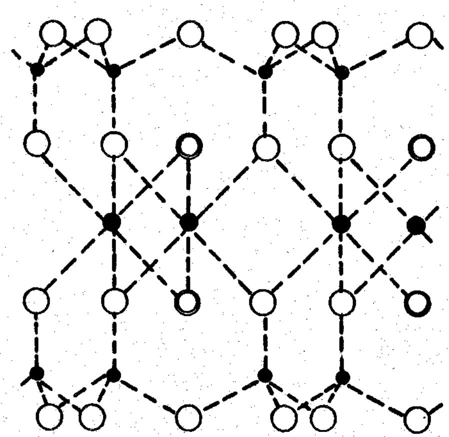

6	O				-12
4	Si				+16
4	O	+	2	OH	-10
4	Al				+12
4	O	+	2	OH	-10
4	Si				+16
6	O				-12

(b) Kaolinite structure

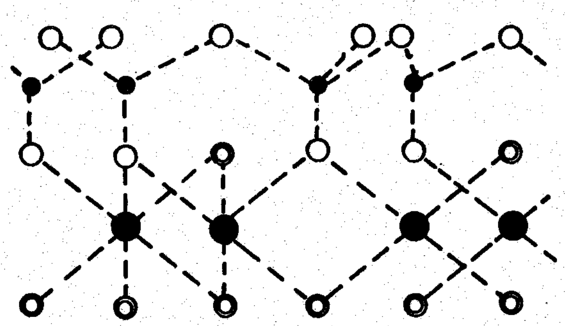

6 O	- 12
4 Si	+ 16
4 O + 2 OH	- 10
4 Al	+ 12
6 OH	- 6

All atoms have been projected into one plane.

● = Si^{+4}
⬤ = Al^{+3}
○ = $O^{=}$
◎ = OH^{-}

groups on either side; therefore, it has no hydrogen bonding between platelets. However, water molecules between the crystals will produce hydrogen bonding and cause the crystals to adhere together, although not nearly so tightly as those of kaolin.

The Concept of Swelling and Non-swelling Clay Minerals and Base Exchange

The pyrophyllite crystal is electronically neutral. If, however, isomorphic substitution of Al^{+++} for Si^{+4} takes place in the tetrahedral layer; there is a deficiency of one positive charge for each substitution. The same is true for isomorphic substitution of Mg^{++}, Fe^{++}, or Li^{+} for Al^{+++} in the octahedral layer. The deficiency is balanced by the addition of a cation electrostatically bonded to the crystal at sites on the flat surface of the crystal. These interlayer ions therefore lie between the crystal platelets in an aggregate of clay mineral crystals. The positions of interlayer cations are called exchange sites.

Cations differ in the ease with which they can be replaced from exchange sites on clay minerals. Obviously, the higher the valence, the stronger the bond and the more difficult to replace, such as Ca^{++} vs Na^{+}. The larger the ionic potential (charge/radius) the stronger the bond, for example $Na^+ > Cs^+$. The higher the concentration of a particular cation in solution the more the driving force towards replacing a cation of lower concentration.

Clay minerals in a solution such as sea water with varying concentrations of different species of cations will reach an equilibrium value for the ratios of the cations on the exchange sites that reflects these forces. In the case of Na^+ vs Ca^{++}, bond strength favors Ca^{++} but concentration favors Na^+ with the result that both are found on the exchange sites in nearly equal amounts (25, p. 683-708).

The order of bond strength for the monovalent cations of the alkali family, which is also the inverse of the order of the ionic radii, is: (20, p. 143-146)

$$Li^+ > Na^+ > K^+ > Rb^+ > Cs^+ \quad (3)$$

However, in the case of exchange on 2-1 clay minerals, K^+ is very difficult to replace. The exceptional strength with which K^+ is bound to clay minerals is due to the arrangement of the oxygen atoms on the surface of the clay crystal (Figure 3). They form a hexagonal hole over the exchange site exactly the size of the K^+ ion. K^+ ions fit into these holes so tightly they

FIGURE 3

View of the oxygen surface layer of a 2-1 clay mineral crystal

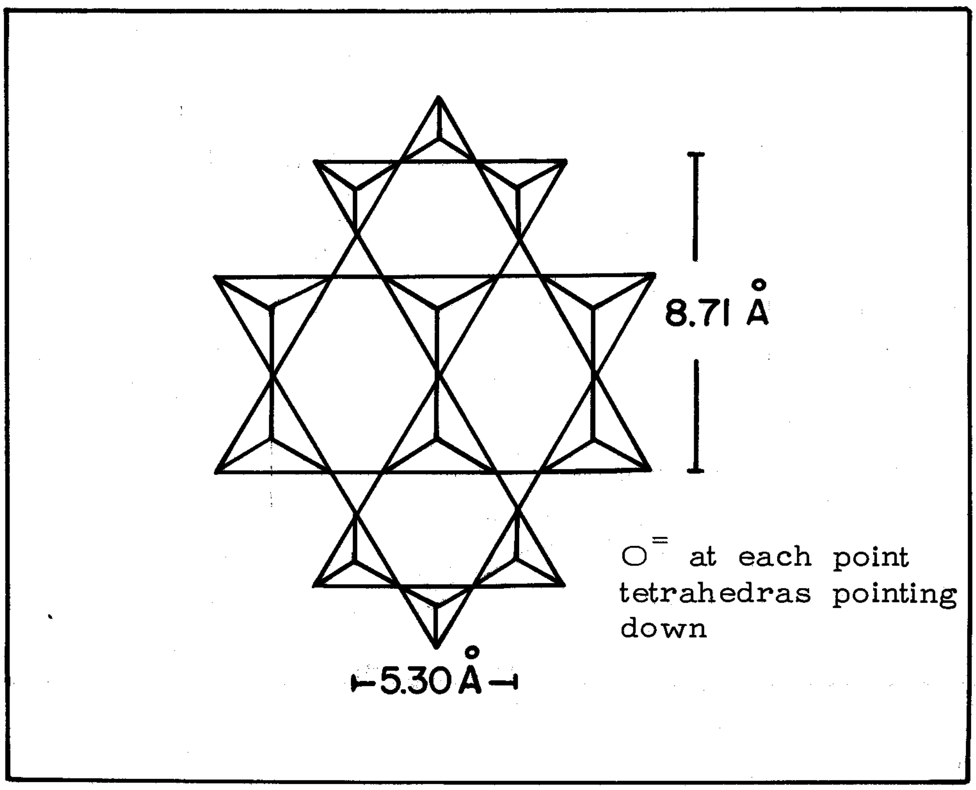

can be removed only with difficulty. Therefore, the K^+ concentration on the exchange sites of marine clay minerals is high although the K^+ concentration in sea water is relatively low.

Isomorphic substitution in the tetrahedral layer places the site of negative charge closer to the position of the exchange ion that substitution in the octahedral layer, thus creating a stronger bond. The number of isomorphic substitutions creates the number of exchange sites. The ion in the exchange site also has an effect upon how close and how tightly the plates are held together. K^+, fitting so tightly in the hexagonal holes, has a tendency to hold the plates so close together that, if there are enough exchange sites saturated with K^+, even water cannot penetrate between the plates. Conversely, the fewer isomorphic substitutions and the larger the number of them in the octahedral layer, the smaller is the required force to pry the platelets apart. Therefore, according to the mode of formation and deposition, 2-1 clay minerals vary from swelling (montmorillonite) to non-swelling (muscovite and biotite) clay minerals, as shown in Figure 4, according to the force required to separate the layers. A complete description of the nomenclature of clay minerals is too long and involved to be included. For those interested, a recent work on this subject is by Charlotte M.

FIGURE 4

Suggested diagenetic relationships in micas

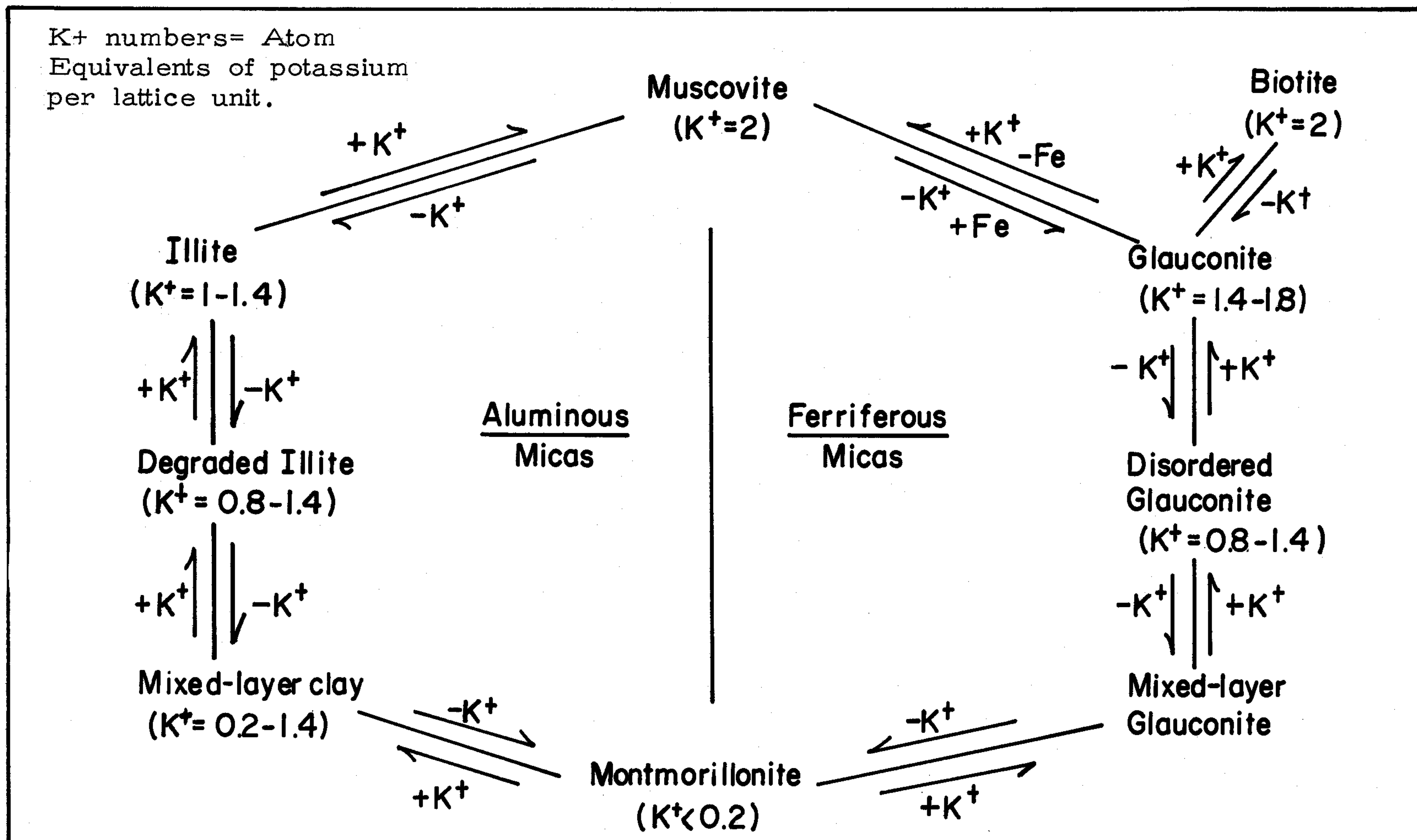

Warshaw and Rustum Roy (44, p. 1455-1492).

Glauconite

Like the word clay, the word "glauconite" plays a dual role in sedimentation terminology. It is a term describing a morphological desposition of clay minerals in the form of pellets and is also the name of a definite class of ferriferous non-swelling clay minerals (Figure 4). Diffractograms of the various ferriferous clay mineral classes are shown in Figure 5. The term has been used so loosely for the name of any pelleted or green clay mineral that, as J.F. Burst (4, p. 310-325) so aptly stated, it has become a wastebasket into which all round or pelleted materials (composition unknown) are placed. The word comes from the Greek glaucos = green, ite = like or greenlike. Therefore, it may be even better to call it the green wastebasket.

The term glauconite, when used correctly, can have a specific meaning. The word glauconite, by itself, signifies a specific ferriferous clay mineral similar in structure to illite. Glauconite is distinguished from illite by isomorphic substitutions of Fe^{+++} for Al^{+++} and Fe^{++} for Mg^{++} in the octahedral layer. Glauconite is, therefore, a non-expanding ferriferous clay

FIGURE 5

Oriented x-ray diffractograms of glauconites

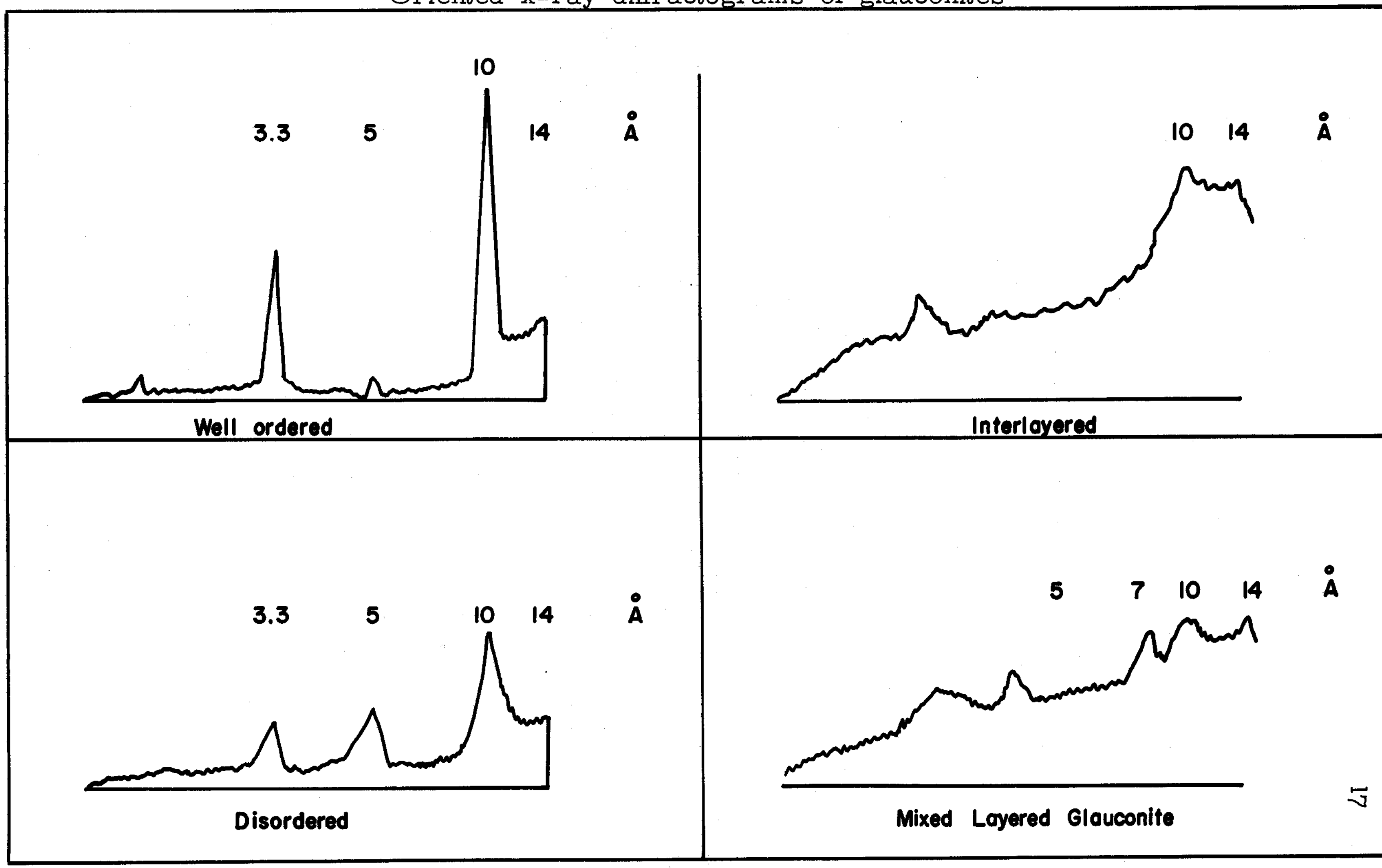

mineral. When the K^+ number as shown in Figure 4 is small enough to allow some expansion, but does not show a sharp 17-18 Å x-ray diffraction peak after solvation like the montmorillonites, prefixes such as disordered, mixed layered or interlayered are used to define the clay mineral as shown in Figure 4. The nonsolvated diffractograms in Figure 5 are also indicative of these gradations. The glauconites can be distinguished from the illites by their greenish color. The color is produced by the Fe^{++} ion in the crystal (8, p. 1-26).

"Glauconite pellets" is the morphological name for any pelleted clay minerals whether they are kaolinite, montmorillonite, chlorite, glauconite or any mixture of these, and whether they are green, brown, gray, blue or black. If these terms are used correctly, then order may be brought out of chaos and the geologist, chemist and oceanographer will understand each other.

Hendricks (25, p. 683-708) has analyzed a large number of samples of glauconite and has described its varying chemical compositions by combinations of the six end formulas shown in Table 1. The representative formulas and isomorphic substitutions possible are shown in Table 2. Table 3 shows the chemical analysis of a glauconite mineral sample.

TABLE I

End formulas for glauconite composition from Hendricks (25, p. 683-708)

	Layer		
	Interlayer	Octahedral	Tetrahedral
(a)	K	$(Fe^{+3}\ Mg^{+2})$	$Si_4O_{10}(OH)_2$
(b)	K	$(Fe^{+3}\ Fe^{+2})$	$Si_4O_{10}(OH)_2$
(c)	K	$(Al^{+3}\ Mg^{+2})$	$Si_4O_{10}(OH)_2$
(d)	K	$(Al^{+3}\ Fe^{+2})$	$Si_4O_{10}(OH)_2$
(e)	K	$(Fe^{+3})_2$	$AlSi_3O_{10}(OH)_2$
(f)	K	$(Al^{+3})_2$	$AlSi_3O_{10}(OH)_2$

TABLE II

Ions in the crystal lattice of 2-1 clay minerals for the formation of glauconite from Hendricks (25, p. 683-708)

(a) Tetrahedral layer

Al^{+3} and Si^{+4} only

(b) Octahedral layer

Al^{+3}, Ti^{+4}, Fe^{+3}, Fe^{+2}, Mn^{+2}, Cr^{+3}, Mg^{+2}, Li^{+}

(c) Interlayer

Li^{+}, K^{+}, Na^{+}, Rb^{+}, Cs^{+}, Ca^{++}, Ba^{++}, Sr^{++}, Mg^{++}

(d) Representative chemical formula for a specific glauconite mineral.

$(K\,Ca_{1/2}Na)_{.84}\,(Al_{.47}Fe^{+3}{}_{.97}Fe^{+2}{}_{.19})\,(Si_{3.65}Al_{.35})$

$O_{10}(OH)_2$

TABLE III

Example of chemical analysis of glauconite from Hendricks (25, p. 683-708)

	Percent	Mole Fraction	Moles
SiO_2	49.4	60.69	Si = .822
Al_2O_3	10.2	50.99	Al = .200
Fe_2O_3	18.0	79.84	Fe^{+3} = .225
FeO	3.1	71.84	Fe^{+2} = .043
MgO	3.5	40.32	Mg = .287
CaO	0.6	28.04	Ca = .021
K_2O	5.1	47.10	K = .108
Na_2O	1.4	31.00	Na = .045

ADSORPTION THEORY

Adsorption and Surface Area Measurements

Adsorption is defined as the concentration of gases, liquids or dissolved substances on the surface of a solid. This study is concerned only with adsorption at a gas-solid interface which is specifically called gas adsorption. Adsorption may involve two distinct types of interactions. One, called chemisorption, is the result of primary valence forces between the interacting substances. It is a true chemical reaction and usually is accompanied by the evolution of a large amount of heat (45, p. 36-39). The other and more general type of adsorption, called physical adsorption, is the result of the formation of van der Waals bonds (usually dipole-induced dipole or dipole-dipole bonds) (45, p. 36-39). Physical adsorption may be considered to be the condensation of a gas on a solid surface with the evolution of small amounts of heat.

From the mathematical expressions for physical adsorption proposed by Langmuir (31, p. 1139-1167) and from their own experimental data, Brunauer, Emmett and Teller (3, p. 309-313) derived an isothermal equation for multimolecular layer adsorption of gases by solids at low temperatures. Emmett, Brunauer and Love (17, p. 57-65) reported the use of physical adsorption for the measurement of the surface area of soils and soil colloids the same year. From these beginnings the Brunauer, Emmett and Teller (B.E.T.) theory, stating that the same forces that produce condensation are also responsible for multimolecular adsorption, was developed. Derivation of the B.E.T. equation results in the following expression for the first monolayer of gas adsorbed on the surface of a solid:

$$\frac{P}{V(P_o - P)} = \frac{1}{V_m C} + \frac{C - 1}{V_m C} \cdot \frac{P}{P_o} \tag{4}$$

Where P = measured pressure

P_o = condensation pressure

V = volume adsorbed at pressure P

V_m = volume adsorbed to form a monolayer

C = thermodynamic constant related to heat of adsorption and heat of condensation by the expression

$$C = \exp^{-} \frac{\Delta H_a - \Delta H_e}{RT}$$

Where ΔH_a = heat of adsorption and ΔH_e = heat of condensation.

If a plot of $\frac{P}{V(P_o - P)}$ vs $\frac{P}{P_o}$ is made from experimentally obtained values, a straight line is obtained for the values of $\frac{P}{P_o}$ between 0.05 and 0.35 for any system that fits the B.E.T. theory. The slope of the line is $\frac{C-1}{V_m C}$ and the intercept is $\frac{1}{V_m C}$. Solving these two equations gives:

$$V_m = \frac{1}{\text{Intercept} + \text{Slope}} \tag{5}$$

From the value of V_m the number of molecules forming the monolayer can be calculated. Then using the cross-sectional area of the molecule determined by other means, the surface area per unit weight of a substance can be calculated (22, p. 1366-1373; 32, p. 447-458).

An alternate method for determining the surface area of a solid from adsorption isotherms has been offered by Harkins and Jura (22, p. 1366-1373). In their development there is no need to assume the molecular area of the adsorbate, which in some cases may be questionable. The two methods show remarkable agreement, however. This speaks well of both theories, since they are based on entirely different principles, the B.E.T. method being based on kinetic theory and the Harkins-Jura method on thermodynamic theory (15, p. 1784-1789).

Harkins and Jura (23, p. 1362-1366) also determined surface areas by what is called the absolute method, based on the measurement of the heat evolved when a surface is eliminated by adsorption of a gas. This method again is in agreement with the B.E.T. theory.

Multilayer Adsorption and Capillary Condensation

As the pressure of a gas in contact with a solid is increased the weight of the gas adsorbed (or condensed) on the solid surface increases. The increase in weight continues beyond the point where a monomolecular layer is formed. The increase in weight is the result of one or both of the two phenomena: (1) Multilayer adsorption or the addition of second, third, fourth and more layers of the gas upon the surface of the solid; and (2) Capillary condensation or filling of pores or cracks in the particles.

Multilayer condensation has been investigated independently by Frenkel, Halsey and Hill (38, p. 1184-1187) on free surface materials (materials containing no capillaries). The conclusion drawn from these investigations and from earlier work by Harkins and Jura on the decrease of energy with the thickness of the film (21, p. 919-927) is that multilayer condensation is independent of the substrate and is only a function of pressure, temperature and the adsorbing gas. The equation called the Frenkel-Halsey-Hill equation (F.H.H.) expresses this relationship isothermally as (38, p. 1184-1187):

$$(6) \qquad (n)^s = \left(\frac{V}{V_m}\right)^s = \frac{K}{\log \frac{P_o}{P}}$$

where n = number of statistical layers

V_m = volume adsorbed for a monolayer

V = volume adsorbed at P

P = pressure

P_o = condensation pressure

s and K = constants depending upon the gas adsorbed.

For nitrogen gas s = 2.75 and K = 1.305 (37, p. 1076-1079). Figure 6 shows the relationship of n vs $\frac{P}{P_o}$ for nitrogen according to the F.H.H. equation.

Capillary condensation is a phenomenon occuring in materials having pores, holes, cracks, or irregularities in the surface and between small particles (37, p. 1076-1079). When a gas is condensed in a pore there is an attractive force from the walls of the pore on all sides of the gas molecule, therefore, more layers will condense at a given pressure within a pore than upon a free surface.

Non-free surface adsorption will therefore reflect both

FIGURE 6

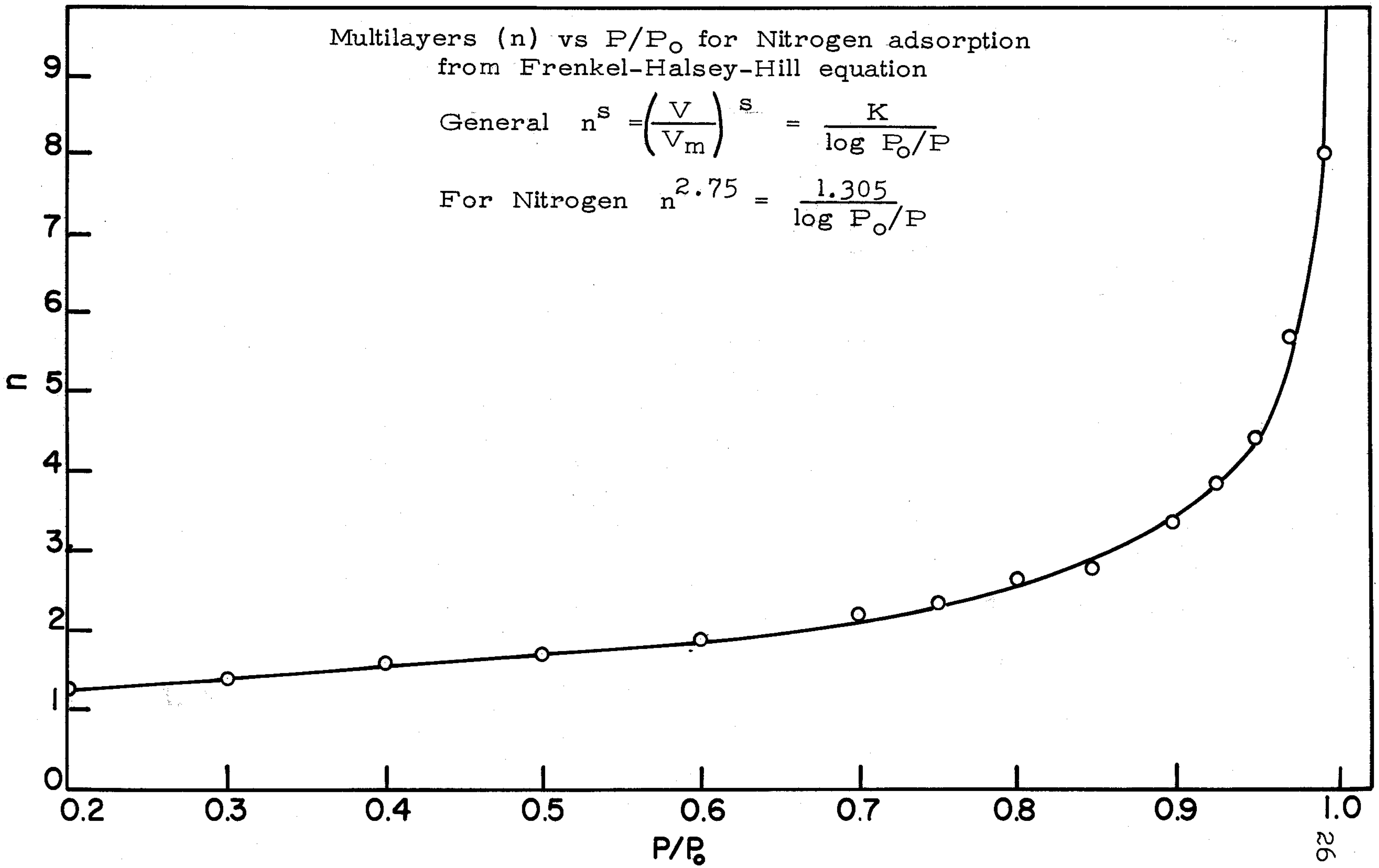

Multilayers (n) vs P/P_o for Nitrogen adsorption
from Frenkel-Halsey-Hill equation
General $n^s = \left(\frac{V}{V_m}\right)^s = \frac{K}{\log P_o/P}$
For Nitrogen $n^{2.75} = \frac{1.305}{\log P_o/P}$
n
0
1
2
3
4
5
6
7
8
9
0.2
0.3
0.4
0.5
0.6
0.7
0.8
0.9
1.0
P/P_o

multilayer adsorption and capillary condensation and the F.H.H. equation does not hold. Instead, the total adsorption can be expressed as follows:

(7) $$V = V_c + nV_m$$

where V_c = the volume held by the pores

n = statistical layers from F.H.H. equation

V_m = volume to form a monolayer on a free surface

The Desorption Isotherm and Pore Size Distribution

Adsorption and desorption isotherms coincide on non-porous materials but on materials having pores or cracks in the surface the desorption isotherm will lag behind. The resulting adsorption-desorption hysteresis may be caused by capillary condensation, rearrangement of the crystal lattice, or a swelling effect. Hirst (26, p. 22-28) attempted to construct models to explain the various forms of hysteresis. He states that if there are regions within a swelling solid where the surfaces are sufficiently close together for surface forces to contribute appreciably to the cohesion of the solid it can be predicted from a mechanical picture that there will be hysteresis. This could be the cause of the hysteresis shown by a swelling laminar structure such as in montmorillonite clay minerals.

When it can be established that the hysteresis is caused by capillary condensation the desorption isotherm can be used to calculate the pore size distribution.

The Kelvin equation (34, p. 268) is the basic mathematical expression used to calculate the pore radius of a pore desorbed at a given pressure:

$$R_k = \frac{2\gamma V \cos\theta}{2.303\ RT\log \frac{P_o}{P}} \tag{8}$$

where γ = surface energy of adsorbate

V = molal volume of gas adsorbed

R = gas constant, 8.316×10^7 erg/deg/mole

T = absolute temperature

P = desorption pressure

P_o = condensation pressure

θ = the contact angle, assumed to be zero

This equation is based on the fact that the condensed material in a pore forms a concave meniscus at the mouth of the pore and the pressure over a concave surface is less than the pressure over a flat surface. R_k is the radius of curvature of the meniscus which is also the radius of the pore.

The Kelvin equation, however, does not take into account the multilayer adsorption upon the walls of the pores and thus gives values too small. The Wheeler equation (2, p. 373-380) makes the correction by adding the thickness of the multilayer to R_k in the relationship:

(9) $$R_p = R_k + t$$

where R_p = radius of pore

R_k = Kelvin radius

t = n x d

where n = statistical number of layers from F.H.H. equation

d = thickness of the adsorbed molecule

Using the Wheeler equation and correcting for multilayer adsorption, Pierce (36, p. 149-152) developed a method for calculating the distribution of pore radii from desorption isotherm data for low temperature adsorption of nitrogen gas. The method is valid when hysteresis is due to capillary condensation, and for pore radii between 20 and 300 Å (39, p. 64-68).

Pore size distributions have also been calculated by forcing a non-wetting material such as mercury into the pores by pressure (13, p. 780-785; 40, p. 223-229). The two methods confirm each other within the range of pores where each method is valid (10, p. 1417-1419). These results are evidence of the validity of pore size distributions calculated from a desorption isotherm. They also are evidence that the structure of the material is not altered by either high or low pressures.

Microstructure Measurements of Marine Sediments

With the use of gas adsorption techniques to measure surface areas and pore volume and size distributions, and taking advantage of x-ray analysis for clay mineral identification and expansion properties, the microstructure of marine sediments can be defined. From data obtained by these techniques adsorption properties can be predicted. The stability of the sediments to morphological changes can be inferred and clues to the mode of deposition can be derived.

EXPERIMENTAL METHODS AND APPARATUS

Description of Adsorption Apparatus

The adsorption and desorption isotherms were determined gravimetrically on an adsorption balance of the type first described by McBain and Bakr (33, p. 690-695) and shown diagramatically in Figure 7. Two reservoirs, one for liquid storage and one for gas storage, are located on the main manifold for easy addition of adsorbate. The manifold is fitted with standard pressure measuring devices: a mercury manometer, an oil manometer filled with Dow Corning 703 fluid, and a McLeod guage. Connected to the manifold is a secondary manifold that accommodates eight adsorption columns, each fitted with an individual stopcock so they can be isolated from the system.

The adsorption balance springs were small quartz helices, each with a sensitivity of about one mm extension per mg load and with a capacity of 400 mg. The samples were contained in small buckets shaped from a piece of tin foil 2 x 5 x 0.0005 cm. Bails made from 0.0056 inch diameter beryllium-copper wire were fitted to the buckets and the tare bucket weight was about 110 mg. The buckets were suspended

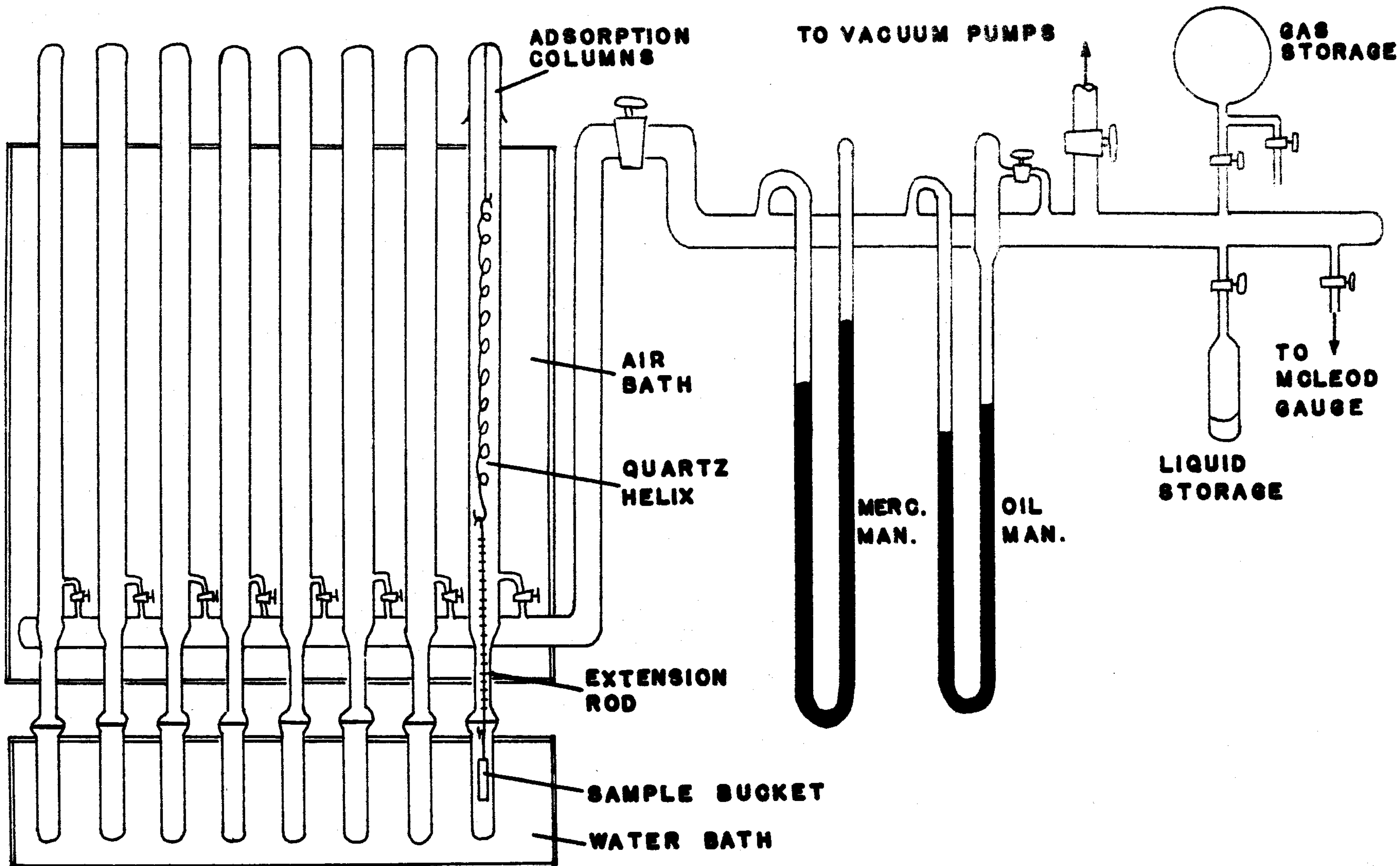

FIGURE 7 Gravimetric Adsorption Balance

from the quartz helices by glass fibers with coded colored markings on them for measurement purposes. The hangers weighed approximately 50 mg. The total weight of bucket and hanger was about 160 mg and, since the maximum load for the springs was 400 mg, the sample weight was between 200 and 225 mg.

The adsorption columns, containing the springs, were enclosed in a constant temperature air bath maintained at 28° ± 0.5° C. The lower portions of the adsorption columns enclosing the sample buckets were kept in a constant temperature water bath for runs near room temperature and were maintained within ± 0.1°. For low temperature nitrogen runs, the water bath was replaced by Dewar flasks containing liquid nitrogen, the temperature having been determined with a vapor pressure thermometer charged with argon. At the temperature of liquid nitrogen (-196°C) the equation describing the vapor pressure curve for solid argon (34, p. 179),

$$\log P_s = \frac{-408.15}{T} + 7.5741, \tag{10}$$

which is valid between 65° and 84° K, was used.

The spring extensions were magnified optically, projecting the coded markings of the suspension rods upon a wall chart about seven feet from the sample tubes. Each spring was calibrated by adding known weights, and a spring constant was calculated in mg per scale division on the wall chart. The sensitivity of the extension readings was about 0.16 mg per scale division and the scale could be read to 0.25 divisions for an overall sensitivity of $\pm$ 0.04 mg for a 200 mg sample. Therefore, the overall sensitivity for a gram of sample was $\pm$ 0.2 mg.

X-Ray Diffraction Apparatus

X-Ray diffractograms were made with a North American Phillips Co. (Norelco) diffraction spectrometer equipped with a Geiger-Mueller tube and Brown recorder. The radiation was Cu_{K_α} (λ = 1.54050 Å). The scanning speed was 1 degree (2θ) per minute for all samples. A one degree divergence and scattering slit combined with the 0.006" receiving slits were found to be most advantageous for optimum peak heights. On the recorder the rate meter settings of 16 x 0.6 corresponding to 480 counts per second full scale with a time constant of 4 proved most successful for optimum peak heights.

Magnetic Separation Apparatus

The machine used for magnetic separation was a Franz Isodynamic Magnetic Separator which is designed to separate ferromagnetic particles from non ferromagnetic particles. The particles pass under an electromagnet by means of a chute and the magnet and chute are mounted on two swivels allowing the pitch and the horizontal orientation to be adjusted. The current flow into the magnet is adjustable, thus providing control of the magnetic flux.

When pitch, horizontal angle and magnetic flux are properly adjusted, ferromagnetic materials moving under the magnet will migrate to the high side of the chute while non-ferromagnetic materials migrate to the lower side. At the end of the chute a divider separates the two portions of the sample into individual containers.

Sampling

The sediment samples used for this investigation were all taken from a small section of the continental terrace near Newport, Oregon. Figure 8 is a bathymetric chart of the section which lies between 44°20' N and 45°00' N and offshore

FIGURE 8

Bathymetric chart of the continental terrace off the coast of Oregon near Newport from 44°20' N to 45° N and off shore to an average depth of 200 fathoms at 124°50' W.

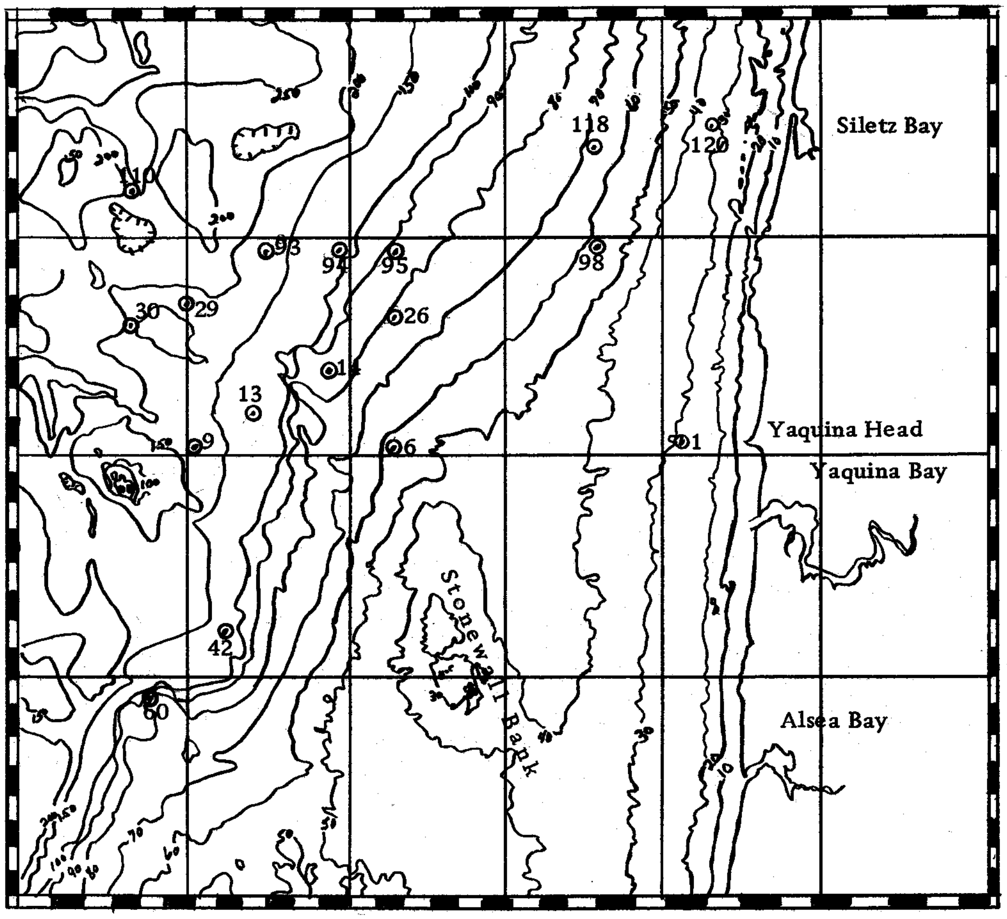

CONTOUR INVERVAL

0-100 fathoms = 10 fathom interval
Over 100 fathoms = 50 fathom interval

STATUTE MILES

0 1 2 3 4 5

to an average depth of 200 fathoms at 124°50' W (7, p. 65-70). The samples were collected with a grab sampler on R/V Acona during cruise No. 6107, July, 1961. The samples were sealed in wide-mouth jars and preserved until analysis.

Sample Preparation

Extractions. In preparing for adsorption measurements, only one of the following procedures was used on any individual portion of a sample.

Soxhlett Extractions. A ten g sample was placed in a porous cup and inserted into a soxhlett extractor. Two hundred ml of solvent was added and recycled for 24 hours. Water, isopropyl alcohol, acetone and diethyl ether were used as the solvent on various samples.

Electrodialysis. A ten g sample was placed in a Mattson cell (dimensions 10 x 20 x 2.5 cm) with 400 ml of distilled water and stirred constantly. The 10 x 20 cm sides of the cell were sheets of untreated cellophane which served as the semipermeable membranes. The outer sides of the membranes were in contact with distilled water in separate chambers. Water flowed through these outside chambers at the rate of 2 l per hour. With a platinum cathode in one container and a copper anode in the other, electric current at no more than 25 ma was allowed to flow through the system. Each sample was electrodialyzed for 24 hours.

Mixing with Solvent. A ten g sample was added to 300 ml of solvent and the mixture stirred for 3 hours. Sea water, distilled water and isopropyl alcohol were used as the solvent on various samples.

Filtration. All extracted samples were vacuum filtered through a medium size sintered glass filter.

Heating and Drying. All samples were dried in a vacuum oven at the desired temperature for a 24 hour period. The pressure was kept as low as possible with a mechanical vacuum pump (about 2 mm of Hg), and the temperatures were 40°, 80°, 95° and 124° for various samples.

Particle Size Standardization for Adsorption Measurements. All samples, after drying, were hand ground with a mortar and pestle until they passed through a 170 mesh sieve (88 μ openings).

X-Ray Diffraction Preparation. Portions of samples after drying and grinding to pass through a 170 mesh sieve (88 μ

openings) were prepared for oriented x-ray diffractograms for clay mineral identification as follows (28, p. 171-240): A portion was saturated with Ca^{++} ions by stirring 0.1 g with 20 ml of 1 N $CaCl_2$ in a plastic centrifuge cup. The sediment was separated by centrifugation and the supernatant liquid poured off. This procedure was repeated four times and the sample was washed three times with distilled water. A second portion was saturated with 1 N KCl in the same fashion. A third portion was stirred with distilled water and centrifuged to aid in orientation of the clay crystals but the natural interlayer ions remained intact.

After cation saturation procedure, a slurry of each preparation was spread onto a glass slide and allowed to dry at room temperature until all surplus moisture was removed. The slides were then placed in a drying oven at 40° C for four hours. The samples were then analyzed by x-ray diffraction.

For further study of the expansion and contraction of the (001) spacings the K^+ saturated portions were heated at 100° for two hours and examined. They were then heated to 550° and again examined by x-ray. The Ca^{++} saturated slides were solvated with ethylene glycol and examined. One sample retaining its natural interlayer ions was solvated and examined and another heated to 550° and examined.

Adsorption-desorption Measurements

The vacuum balance used in this investigation was equipped to measure 8 samples simultaneously. This allowed larger numbers of samples to be measured and insured better comparison when several samples were examined simultaneously under the same conditions (Figure 7).

Approximately 200 mg of each sample was weighed and placed in the tin buckets and attached to the hanger of a quartz spring in an adsorption column (Figure 7). The samples were outgassed for 36 hours at 10^{-4} cm pressure and at room temperature. The apparent loss in weight measured by the adsorption balance was subtracted from the original weight of the sample. Therefore, the sample weights were recorded "in vacuo" after outgassing.

Adsorption-desorption isotherms were made with nitrogen at -196° C allowing 15 to 20 minutes to reach equilibrium at each step. Adsorption isotherms were made with water vapor up to P/P_o of about 0.5 at 25°, allowing 1 hour for equilibrium at each step.

Accurate pressure readings presented some problems, especially with water whose saturation pressure near room temperature is quite small. An optical system projected the mercury manometer on a screen about 17 feet away and this projection gave an overall magnification factor of 26.5. The pressure could be read to $\pm$ 0.05 mm Hg.

Magnetic Separation Procedure

The fraction of the sample having particles with diameters greater than 62 μ were removed by wet sieving with a 230 mesh sieve (62 μ openings). The coarse fraction was oven dried at 40° C. The ferromagnetic particles were separated from the coarse fraction (above 62 μ) after drying by means of the Franz Isodynamic Magnetic Separator described on p. 35 and the percent of ferromagnetic material in the coarse fraction determined. No separation of the clay and silt size was made (6).

CALCULATIONS AND MINERAL IDENTIFICATION

Surface Area Calculations

Surface areas were determined by linear B.E.T. plots (see p. 21) between $P/P_o = 0.05$ and 0.35. Plots were made of the function $\frac{P}{W(P_o-P)}$ vs P/P_o. When W is expressed in mg/g the slope and the intercept both are in reciprocal mg, resulting in a value of W_m, the weight of the monolayer, instead of V_m, the volume of a monolayer, as given in the literature for B.E.T. calculations (3, p. 309-319). Since the apparatus gives weight values this procedure eliminates the necessity of converting weight to volume. The number of molecules of gas adsorbed when the monolayer is formed is calculated as follows:

$$N = \frac{6.023 \times 10^{23} \times (W_m)}{M \times 10^3} \tag{11}$$

where N is the number of molecules adsorbed for the monolayer per gram of substrate and M = Molecular weight of gas. N is also called the number of active sites or points where molecules are adsorbed. The surface area was determined by multiplying N by the cross sectional area of the adsorbed gas molecule.

The area used for nitrogen was 16.2 $Å^2$ and for water vapor 10.6 $Å^2$ (18, p. 21-24). For rapid calculations an area constant was calculated for each gas adsorbed by combining N and the cross sectional area of the gas as follows:

$$(12) \quad \text{Area Constant } (m^2/mg) = \frac{6.023 \times 10^{23} \text{ (Area of molecule } m^2)}{M \times 10^3}$$

The area constant calculated for nitrogen was 3.48 m^2/mg and for water vapor 3.55 m^2/mg. Therefore:

$$(13) \quad W_m \frac{mg}{g} \times \text{Area Constant } \frac{m^2}{mg} = \text{Surface Area } \frac{m^2}{g}$$

Figures 9a and b are examples of linear B.E.T. plots of three marine sediment samples with wide variations in surface area. Figure 10 shows the adsorption-desorption isotherms of the same samples. The B.E.T. plots were made from these isotherms.

<u>Sensitivity and Reproducibility of Surface area measurements</u>

The sensitivity of the adsorption balance is ± 0.2 mg/g giving an accuracy of $\pm 5\%$ for a sample having a W_m value of 4 mg/g. Considering errors inherent in extrapolation of values from adsorption isotherm graphs, the accuracy of pressure

FIGURE 9a

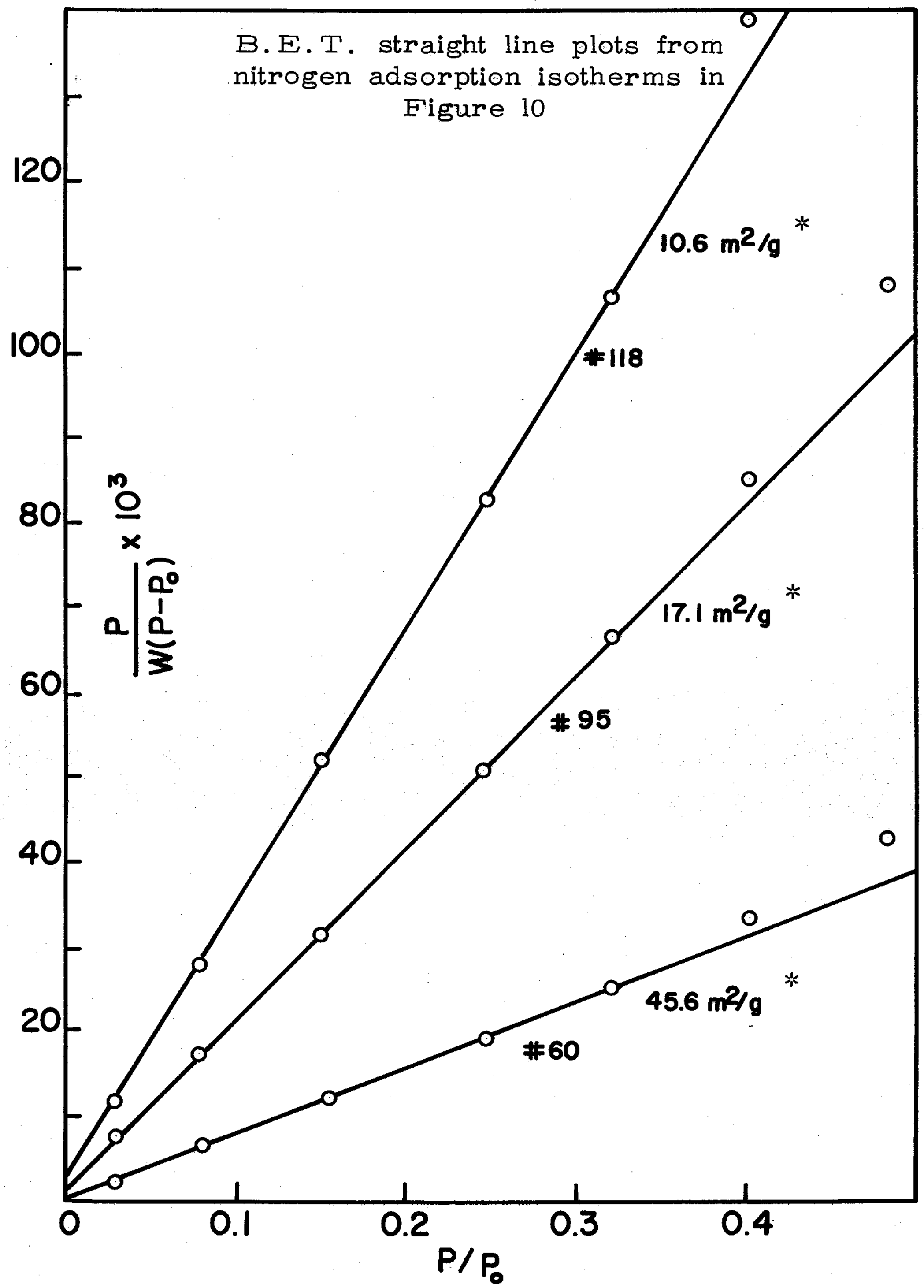

* surface area of sample

FIGURE 9b

B.E.T. straight line plots from water vapor adsorption isotherms in Figure 10

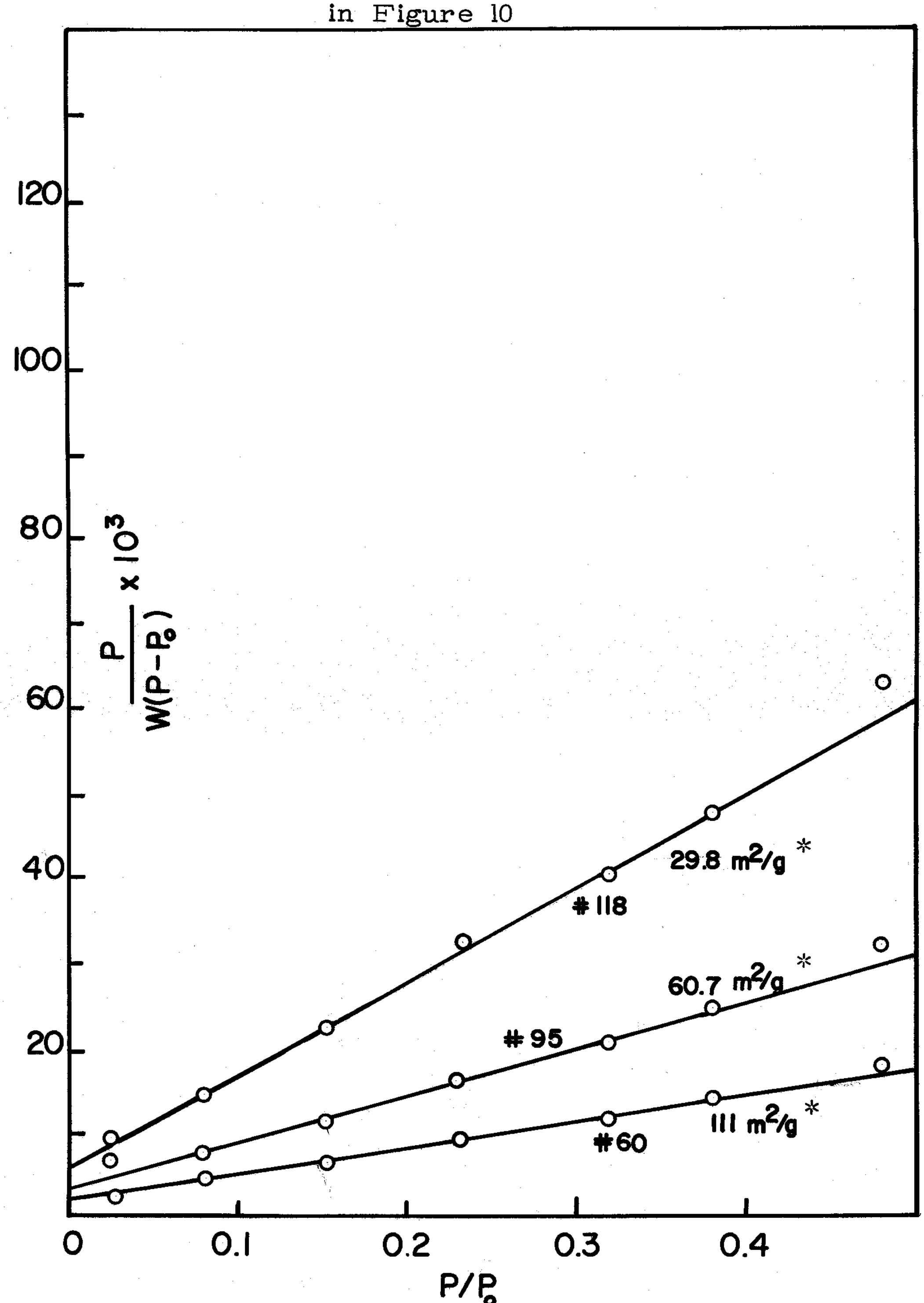

* surface area of sample

FIGURE 10

Adsorption-desorption isotherms on terrigenous marine sediments

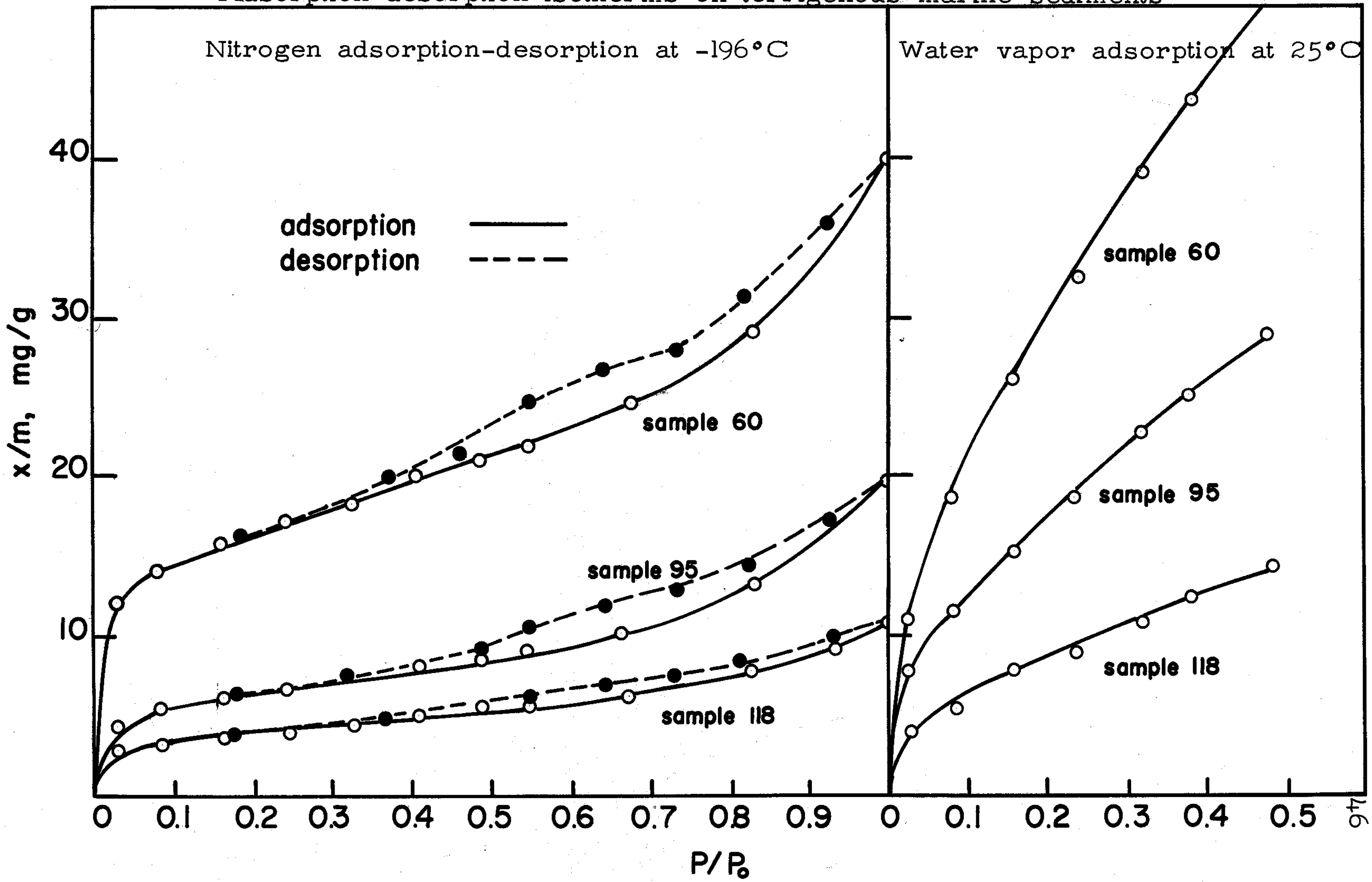

readings, fluctuations in temperature, possible nonlinearity of the spring constant and change in lens focus due to movement of the spring, the real test of precision was the reproducibility of results. It was found that for any sample having a W_m value over 4 mg/g, reproducibility was always within ± 5%. Between 4 mg/g and 3 mg/g all results were within ± 7%. Between 3 mg/g and 1 mg/g all results were within ± 10%. Below 1 mg/g there was very little reliability to the results obtained.

All surface area values reported are the result of two or more measurements on any individual sample and all were reproducible within the above limits.

Pore Sized Distribution Calculations

The distribution of pore volume as a function of the pore radii was calculated from the nitrogen desorption isotherm by assuming the observed hysteresis was due to capillary condensation. Thirty increments from $P/P_o = 1$ to $P/P_o = 0.352$ were used. For each value of P/P_o the weight adsorbed (W) was extrapolated from the isotherm as shown in Appendix 1.

At each increment the Kelvin pore radius was calculated from the Kelvin equation (see p. 28):

$$(14) \qquad R_K = \frac{2\,\gamma V \cos\theta}{2.303\ RT} \cdot \frac{1}{\log P_o/P} = \frac{4.14}{\log P_o/P}$$

where $\frac{2\,\gamma\ V \cos\theta}{2.303\ RT} = 4.14$ for nitrogen at -196° (36, p. 149-152) and R_K is the Kelvin radius (see p. 28). The correction value for multilayer adsorption (t) as given by the Wheeler equation is (see p. 29):

$$(15) \qquad R_p = \frac{4.14}{\log P_o/P} + t$$

where t = nd (see p. 29). The F.H.H. equation (see p. 25) was used to determine n, the number of layers adsorbed, for each increment and the thickness of the adsorbed nitrogen molecule was assumed to be 3.6 Å (36, p. 149-151; 38, p. 1184-1187).

Inspection of desorption isotherms of the marine sediments showed a sharp dip in the curve between $P/P_o = 0.6$ and 0.4. Therefore, the increments were taken closer together through this range in order to define the pore volume maximum more closely.

The volume desorbed from pores (ΔV) per Å (Δr) in each increment was plotted vs the average pore radius ($\bar{r}$) of each increment as shown in Figure 11.

The calculations were performed on a ALWAC No.

FIGURE 11

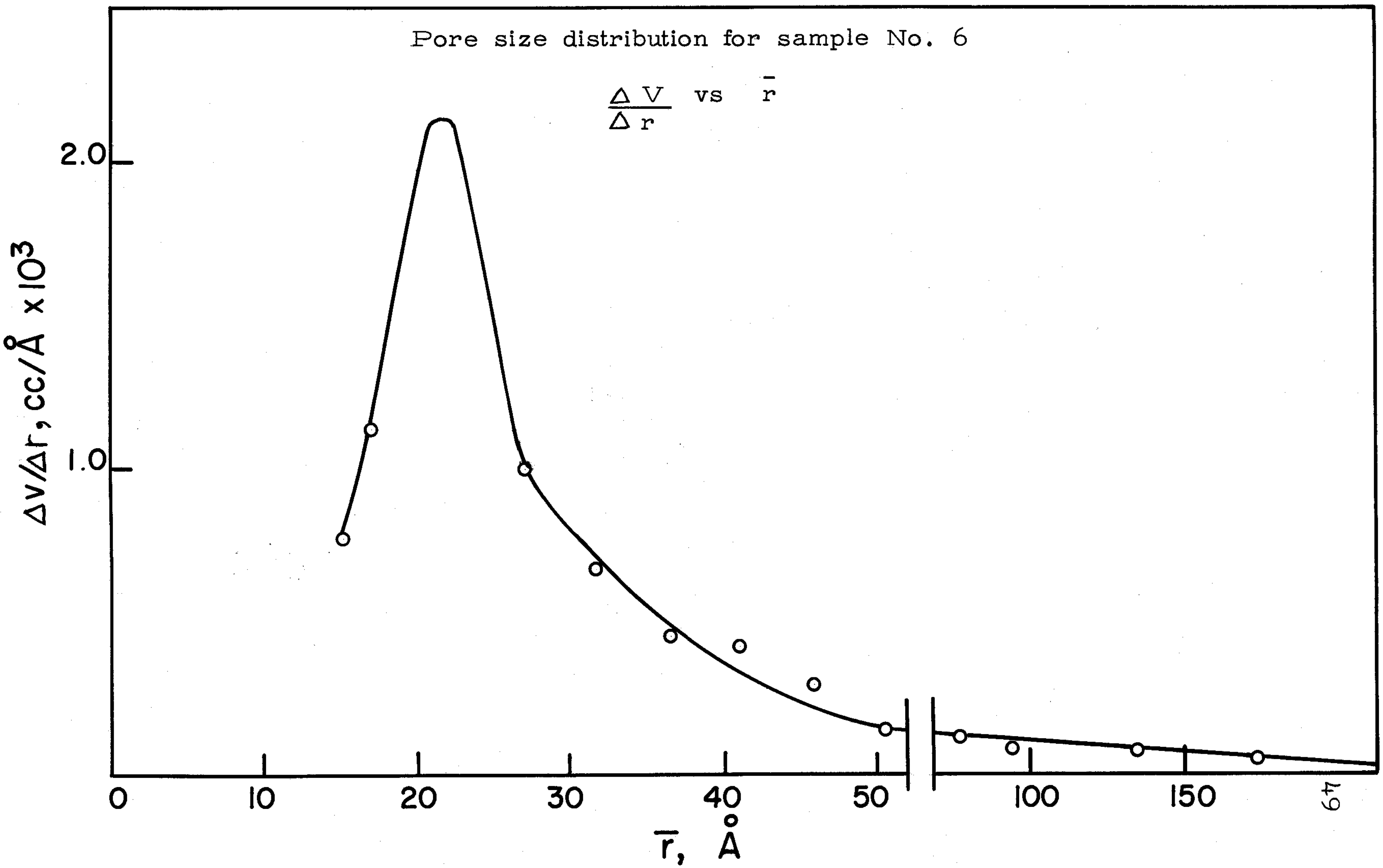

Pore size distribution for sample No. 6

$\frac{\Delta V}{\Delta r}$ vs $\bar{r}$

III E computer. Calculations were made on all samples at the same P/P_o increments, so that it was necessary to feed only W values into the computer for each increment, as shown in Appendix 1. R_K and n, both being functions of P/P_o, were preset in the code for each increment. Appendix 3 is the flow chart of the pore size distribution calculations as performed by the computer. The machine code and instructions for its use are shown in Appendix 4 and an example of the readout is shown in Appendix 2.

X-Ray Diffraction Analysis of Clay Minerals

Low angle x-ray diffractograms of the sediment samples were made between 2° and 14° (2Θ). Clay mineral identification was made by comparing the (001) spacings with the scheme shown in Table 4 (44, p. 1455-1492). Diffractograms from 30° to 2° (2Θ) were also examined to identify quartz and other forms of silica.

TABLE IV

Clay mineral identification by x-ray diffraction measurement of (001) spacings

Clay Mineral	(001) spacings, Å				
	Ca^{++} Saturated	K^{+} Saturated	Ca^{++} Saturated solvated with ethylene glycol	K^{+} Saturated, heated 100°C	K^{+} Saturated, heated 550°C
2:1 Expanding Clay, Montmorillonite	14-15	12.5 broad	17-18	10.5	10
2:1 Semi-expanding Clay, Vermiculite	14-15	10.5 sharp	14-15	10.5	10
2:2 Non-expanding Clay, Chlorite	14-15	14-15	14-15	14-15	14-15
2:1 Non-expanding Clay, Mica, Illite Glauconite	10	10	10	10	10
1:1 Non-expanding Clay, Kaolinite	7.2	7.2	7.2	7.2	decomposes

EXPERIMENTAL RESULTS AND DISCUSSION

Verification of Reversibility of Adsorption On a Free Surface

When a surface is free of pores, cracks, or irregularities which produce capillary condensation, the desorption isotherm should follow the adsorption isotherm. For the purpose of verifying this reproducibility anatase (TiO_2) was used. Anatase is well established as a free surface powder. As is shown in Figure 12, the adsorption and desorption isotherms do in fact coincide. There is no evidence of hysteresis. The absence of hysteresis in the anatase isotherm also eliminates the possibility that hysteresis is caused by the apparatus or the techniques.

Surface Area Measurements on a Free Surface with nitrogen and water vapor

The water molecule has a large dipole moment while the dipole moment of the nitrogen molecule is zero. Thus when water vapor is adsorbed it produces a stronger bond with the substrate than does nitrogen. The water molecule bonding strength allows it to penetrate into smaller pores and to expand laminar clay mineral platelets and therefore show a

FIGURE 12

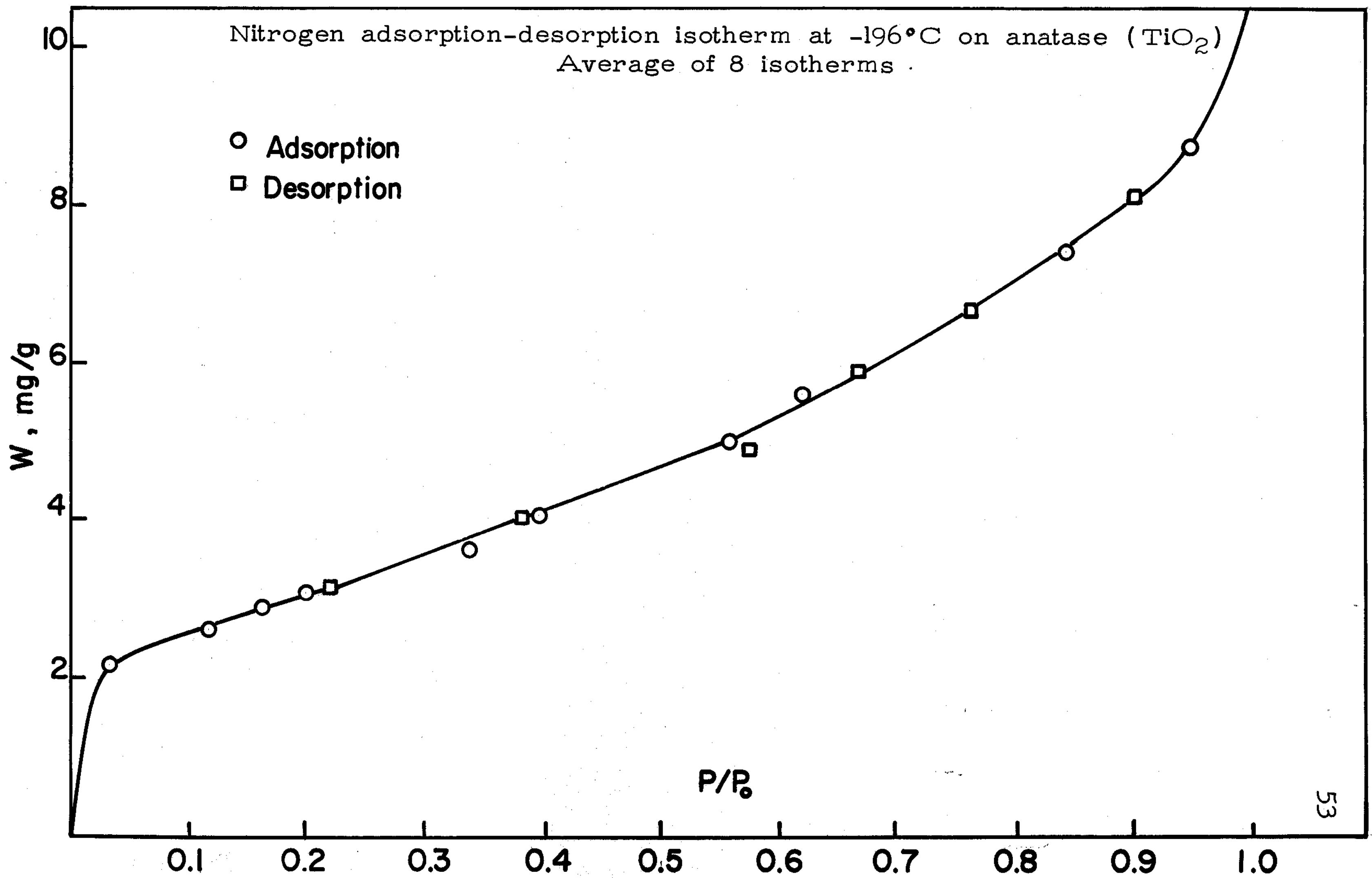

Nitrogen adsorption-desorption isotherm at -196°C on anatase (TiO2)
Average of 8 isotherms
Adsorption
Desorption
W, mg/g
P/Po
10
8
6
4
2
0.1
0.2
0.3
0.4
0.5
0.6
0.7
0.8
0.9
1.0

larger B.E.T. surface area on these materials than nitrogen. However, when a material has only a free surface (a non-porous surface) both gases should give the same B.E.T. surface area. This was verified experimentally with anatase. The average nitrogen surface area measured for eight samples was 8.70 m^2/g ± 10% and the average for the same eight samples measured with water vapor was 8.91 m^2/g ± 10%. These results are well within the experimental error of ± 10% for a material having a W_m value below 3 mg/g in view of the sensitivity of the apparatus.

Verification of the Frenkel-Halsey-Hill Equation

The F.H.H. equation states that the number of layers of adsorbed gas (n) is independent of the substrate and dependent only upon the gas adsorbed and the relative pressure, expressed mathematically (see p. 24):

$$n^s = \frac{K}{\log P_o/P} \tag{16}$$

If a material had only a free surface and if the above relationship is true, then for any gas for which s and K are known, W_m could be evaluated at any P/P_o value by the following relationship:

(17) $$W_m = \frac{W}{n}$$

where W_m is the weight of a monolayer, W is the weight adsorbed at P and n is the F.H.H. number of statistical layers. A plot of W/n vs P/P_o for nitrogen adsorption on anatase using s=2.75 and K=1.305 is shown in Figure 13. The plot is the average of eight samples. The plot should be linear over the range of P/P_o between 0.2 and 0.9 if no capillary condensation occurs. Above P/P_o of 0.9 deviation can be attributed to condensation between the particles (37, p. 1076-1079). As shown in Figure 13 experimental deviation from the average within the range of 0.2 to 0.9 was within ± 10%. The average W_m value obtained from this method is 8% higher than the B.E.T. value but within the accuracy of the apparatus for low surface area materials.

The Use of W/n for the Determination of Surface Areas of Marine Sediments

Determination of the gas adsorption surface area using the equation:

(18) $$\frac{W}{n} = W_m$$

FIGURE 13

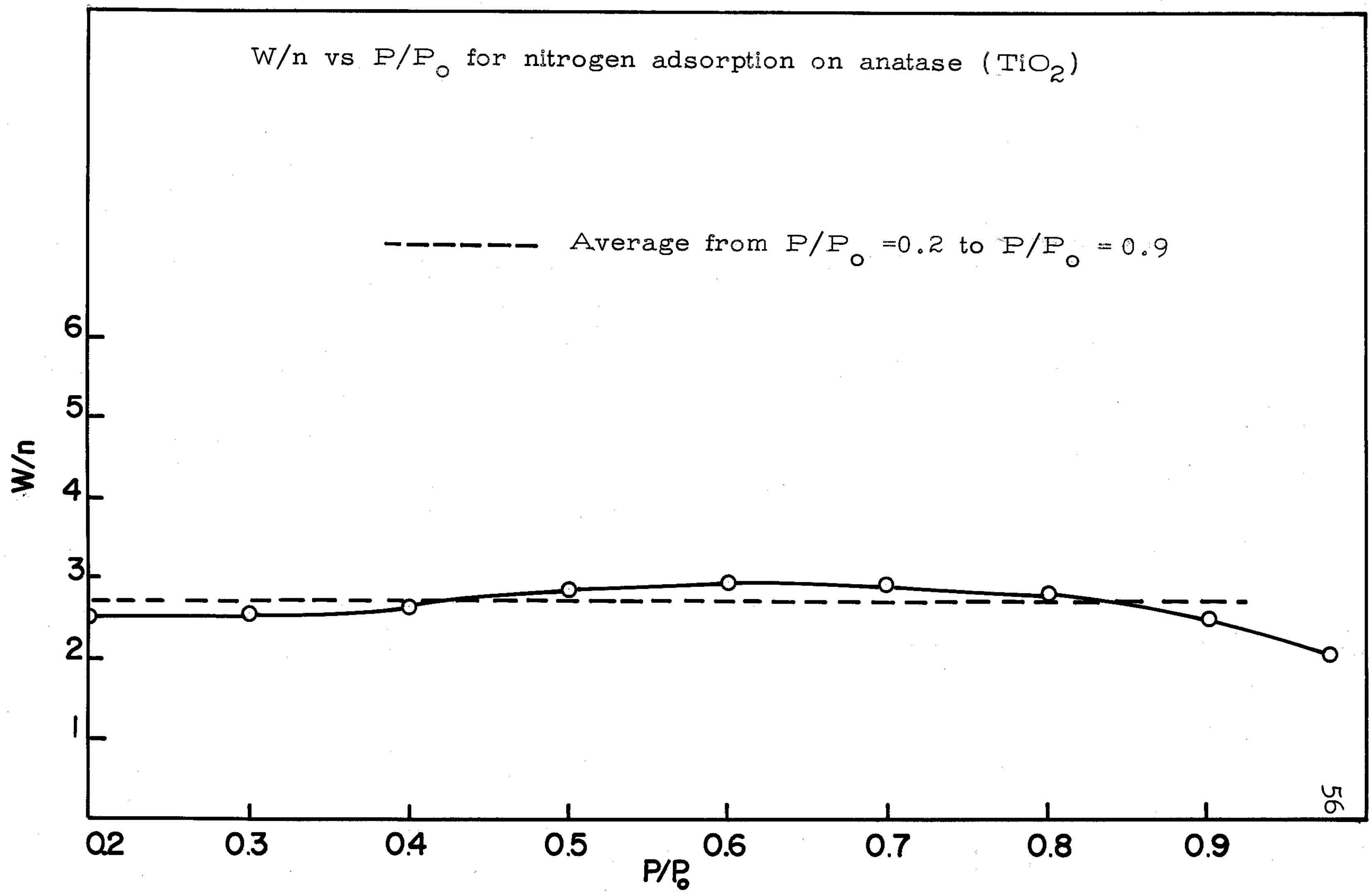
W/n vs P/Po for nitrogen adsorption on anatase (TiO2)
Average from P/Po =0.2 to P/Po =0.9
W/n
6
5
4
3
2
1
0.2
0.3
0.4
0.5
0.6
0.7
0.8
0.9
P/Po

would certainly simplify the calculations compared to B.E.T. plots. The use of this method would simply require measurement of the adsorption at only one pressure. The adsorption balance could be constructed to automatically regulate the pressure at a predetermined amount and allow the system to reach equilibrium. The weight adsorbed could be read and W_m calculated directly from equation 18.

The feasibility of this procedure for nitrogen surface areas was investigated. The P/P_o value of 0.2 (15.2 cm Hg) was selected as the best value to use because (1) it is somewhat above the B point (pressure when the first monolayer is formed), (2) no capillary condensation has occured up to this point, (3) 15.2 cm is a pressure that can be accurately measured, and (4) the n value is still small (1.25). Comparison of W/n values at $P/P_o = 0.2$ with B.E.T. W_m values are shown in Appendix 5 for 45 isotherms of terrigenous marine sediment samples from the area shown in Figure 8. The W/n value averages 1.7% higher than B.E.T. W_m values with no deviations greater than ± 10% except No. 41, a sample with a W_m value too low for the sensitivity of the apparatus. There are only 12 samples showing deviations greater than ± 5%, the reproducibility of B.E.T. measurements.

The results of this investigation speak well for the use of W/n values in any system where it can be applied. It is even possible that the surface areas measured by this method may be as accurate or even more accurate than those taken from B.E.T. plots.

No valid relationship between B.E.T. W_m values and W/n values could be established for water vapor. The difficulty of reading low pressures could be a partial cause of poor correlation between the two values. The possibility of low pressure hydration of cations on the exchange sites of the clay minerals can produce the same effect as capillary condensation. Therefore, W/n values are much higher than B.E.T. W_m values for water vapor. It is also necessary to establish the values of s and K for water vapor before n values can be evaluated. At present these values have not been established for water vapor.

Variation of Surface Areas of Terrigenous Marine Sediments Compared with Natural Parameters. The surface areas of 16 characteristic samples from the region shown in Figure 8 are compared with various other parameters as shown in Table 5. Analysis of Table 5 shows correlation with both depth of

TABLE V

Comparison of various parameters of terrigenous sediments (1) depth and distance from shore (2) ferromagnetic material (3) nitrogen surface area* (4) water vapor surface area* (5) average grain size (6) % silt and sand size.

Color	Sample No.	Mi. from shore	Depth fathoms	% Ferro-magnetic	N_2 surface m^2/g	H_2O surface m^2/g	Avg. grain size	% Under 62 silt and sand
Tan	1	4	30	0.00	2.5	8.2	154	0.00
	13	27	125	7.80	14.0	60.8	31	88
	120	7	30	11.5	3.2	7.8	248	0.00
	98	8	30	15.9	5.5	19.2	158	6
	118	12	70	23.0	10.2	29.4	141	15
	6	21	50	---	40.0	99.5	--	--
Gray	26	19	80	38.8	12.7	42.3	108	32
	42	28	100	42.2	15.2	53.0	58	53
	95	19	90	46.3	17.0	58.0	70	45
	93	27	150	46.3	13.5	48.5	3	88
	30	32	120	47.5	19.2	76.5	5	95
	14	22	90	56.5	14.0	50.8	80	32
Green	94	22	175	73.0	21.9	67.5	74	39
	9	30	200	80.2	33.7	88.4	154	20
	29	30	200	97.0	43.8	115	185	8
	60	33	200	98.0	45.5	113	272	15
	110	34	250	97.0	53.0	125	254	5

* Surface area measurements were made on unextracted samples vacuum dried at 80° and ground to pass through a 170 mesh screen.

sample and distance from shore. In general, surface areas increase with depth and distance from shore. The average particle size decreases with distance and depth to a region 25 miles off shore and a depth of 150 fathoms. Beyond this point the average size of the particles becomes less regular, increasing on the rises and still decreasing in the depressions. The amount of ferromagnetic material in the coarse fraction also shows a general increase with depth and distance from shore (6). The large particles of near shore samples are chiefly quartz sand but the large particles in the deep samples are glauconite pellets (6).

Ferriferous clay minerals as shown in Figure 4 are ferromagnetic and can be separated from other clay minerals and quartz sand by magnetic separation. Table 5 shows an increase in surface area with increase in ferromagnetic materials which indicates that glauconite minerals are an important contributor to the total surface area. The colors of powdered samples also go through a definite change with increasing surface area and increasing ferromagnetic material. Samples 1 and 120 are light tan in color. As the surface area, ferromagnetic material, depth and distance from shore all increase the color changes from light tan through gray to green.

The green becomes more intense as these parameters increase. Dotted lines between 6 and 26 and between 14 and 94 indicate the points where color changes are the most pronounced.

Effect of Temperature on Surface Area Measurements. The effect of temperature on the measurement of surface areas was investigated for the purpose of defining a standardized procedure to produce comparative surface area measurements. The samples must be dried, and it is important to specify the drying temperature. Kulp (29, p. 148-159) reported no measurable change in nitrogen adsorption surface areas with heating up to 340°C. The results of that investigation may be true for pelagic sediments but it is not true for terrigenous sediments. As shown in Table 6 heating above 80° C produces a reduction in the surface area measurements. There was no measurable difference when the samples were dried at 40° and at 80°, but above 80° the surface areas decrease with increasing temperature. X-Ray diffraction measurements indicate that heat partially collapses the clay platelets which can account for the reduction in surface.

For comparative surface area measurements of terrigenous sediments the sample should never be heated over 80°C.

TABLE VI

Effect of temperature on the surface areas of terrigenous marine sediments
Surface areas are expressed in m^2/g

Sample	Heating Temperature (°C)							
	N_2				H_2O			
	40°	80°	95°	124°	40°	80°	95°	124°
26 Dialyzed	20.8	20.6	18.5	14.4	42.2	42.4	42.4	34.0
60 Dialyzed	70.8	69.3	--	58.1	127	113	--	94.0
110 Dialyzed	--	77.0	71.0	--	--	153	143	--
14 Dialyzed	--	24.7	22.6	--	--	68	61.5	--

Effect of Extractions on Surface Area Measurements. Surface area measurements are expressed as m^2/g and indicate nothing about the material contained in the substrate. Terrigenous marine sediments are mixtures of silicate minerals, organic compounds and inorganic compounds. The organic and carbonate content of the sediments in the region of this investigation are low (6). The effect on these measurements of extracting soluble substances from the basic silicate minerals was investigated. Four solvents, water, isopropyl alcohol, acetone and diethyl ether, were selected on the basis of their degree of polarity. Water was the best polar solvent and diethyl ether the best nonpolar solvent used. Soxhlett extractions were performed on sample No. 93 and the results are shown in Table 7.

No quantitative investigation of the material removed by these solvents was made but the following qualitative observations were made:

1. The solution from the sample extracted with water, when evaporated to dryness, produced considerable quantity of white and brown crystals.

2. The solution from the sample extracted with isopropyl alcohol produced considerable quantity of white

crystals with some brown coloration in them. The solution had a yellow coloration before evaporation.

3. The solution from the Acetone extraction, while being evaporated to dryness, turned from bright yellow to green and when it became dry turned black. As evaporation was taking place there was an odor similar to the curing of alfalfa hay. The colors indicated here are the same as Laevastu (30, p. 325-334) found with acetone extractions. The phenomenon is caused by degradation products of chlorophylls according to Laevastu. The final residue was black but many white crystals were also found.

4. The solution from the sample extracted with diethyl ether remained clear but upon evaporation there remained a small amount of yellow wax-like residue.

Inspection of Table 7 shows that the more polar the extraction solvent the higher the resulting surface area. No change is observed with diethyl ether while water extraction increased the nitrogen surface area approximately 50%. This phenomenon suggests that removal of inorganic material affects the total surface markedly by opening up cracks and pores in the silicate minerals and by removal of low surface materials. It also indicates that very little organic material is adsorbed on

TABLE VII

Effect of solvent extractions on the surface area of sample No. 93

Extraction Procedure	Surface Area, m^2/g *			
	N_2	% Increase	H_2O	% Increase over unextracted
a - Soxhlett				
1 - Water	20.7	53	55.0	13
2 - Isopropyl Alcohol	16.9	24	48.8	0
3 - Acetone	16.5	22	49.5	2
4 - Diethyl ether	13.2	0	49.5	2
b - Electrodialyzed	23.3	72	58.7	20
c - Stirred in distilled water	22.9	69	58.4	20
d - Stirred in sea water	13.6	0	49.5	1
e - Unextracted	13.5	--	48.5	--

* Drying temperature 80° C

the surface of the sediment particles. It should be further pointed out that Soxhlett extraction with water yields a 10% lower nitrogen surface area than water extraction by stirring the sediment with distilled water. Inspection of Table 6 shows that this should be the expected result because 95° temperature lowers the nitrogen surface about 10% and for Soxhlett extraction the water is heated to its boiling point, 100°.

Water vapor surface areas are not so markedly affected by extractions when figured as percent but the change in m^2/g is very nearly the same as with nitrogen.

Table 8 shows the effects of heat and extractions on the surface area of sample No. 60. This is a sample with high surface area and high percentage glauconite pellets. The result for sample 60 is similar to sample No. 93.

The highest surface area was obtained on all samples after electrodialysis as shown in Table 9. This process is too severe to be of value. After electrodialysis a considerable quantity of iron oxide and aluminum oxide was found on the semipermiable membrane next to the electrodes and x-ray diffractograms show broadening of the clay mineral peaks on dialysed samples. These phenomena indicate that the electric current is disrupting the crystal structure of the clay minerals,

TABLE VIII

Effect of solvent extractions and heat on the surface area of sample No. 60
Surface areas are expressed in m^2/g

	Drying Temperature					
	40° C		80° C		125° C	
	N_2	H_2O	N_2	H_2O	N_2	H_2O
1) Unextracted	--	--	45.5	113	--	--
2) Soxhlett extracted with isopropyl alcohol	--	--	57.1	123	--	--
3) Stirred with distilled water	60.4	116	63.2	122	55.8	95
4) Electrodialyzed	70.5	127	69.3	123	58.9	97.5

TABLE IX

Surface areas of unextracted sediment samples compared to electrodialysis samples. Drying temperature 80° C.

Sample	Surface Area, m^2/g			
	Unextracted		Electrodialyzed	
	N_2	H_2O	N_2	H_2O
93	13.7	48.5	23.3	58.6
95	17.0	58.0	27.0	64.5
6	40.0	99.5	51.4	135
110	53.0	125	76.0	148
26	12.7	42.3	20.6	42.4
14	14.0	50.8	26.8	64.5
42	15.2	53.0	28.0	64.5
30	19.2	76.5	34.5	77.0

causing them to be disordered and exposing more surface for gas adsorption.

<u>The Effect of Clay Mineral Interlayer Ions on Surface Areas.</u> Three portions of sample No. 60 were prepared, one saturated with Na^+, one with K^+ and one with Ca^{++}, following the procedure for interlayer saturation described under x-ray diffraction preparation (p.38). The nitrogen and water vapor surface areas of these samples were measured and the results are shown in Table 10. When these results are compared with

isopropyl alcohol extraction they show that Ca^{++} saturation increases both nitrogen and water vapor surface areas. The increase is very pronounced with water vapor. K^{+} saturation on the other hand does not affect the nitrogen surface area but markedly reduces the water vapor surface area. Na^{+} saturation shows the same effect as K^{+} saturation but does not reduce the water vapor area so markedly.

TABLE X

The effect of the interlayer cations upon the surface area of sample No. 60. Dried at 80° C.

Preparation	Surface Area, m^2/g N_2	H_2O
(1) Dried and ground without any treatment	45.5	113
(2) Soxhlett extracted with isopropyl alcohol	57.1	123
(3) Interlayer ions Ca^{++} saturated	63.8	149
(4) Interlayer ions Na^{+} saturated	57.9	96
(5) Interlayer ions K^{+} saturated	59.2	85.9
(6) Electrodialyzed	69.3	123

Table 10 shows the effect of the adsorption characteristics of marine sediments produced by a change in the ionic atmosphere of its environment. The ionic concentration of these three ions in sea water is as follows (24, p. 4):

$$Na^{+} = 0.48\ M$$
$$K^{+} = 0.01\ M$$
$$Ca^{++} = 0.01\ M$$

The relative number of moles of Na^{+}, Ca^{++}, and K^{+} on the exchange sites of glauconite minerals are shown in Table 3 as analysed by Hendricks (25, p. 683-708):

$$Na^{+} = 0.045$$
$$K^{+} = 0.108$$
$$Ca^{++} = 0.021$$

The concentration of these cations reflects their sea water concentration and the strength of the bond of each ion to the clay mineral. Sample No. 60 is mostly composed of green glauconite pellets and x-ray diffractograms show them to be mixed layered glauconite minerals (Figure 4). The glauconite clay minerals are formed only in certain marine environments (5, p. 310-325) and therefore the exchange ions must reflect the ionic concentrations of sea water.

X-Rays also show that Ca^{++} saturation expands the clay crystals and produces more disorder while K^{+} saturation draws the clay mineral crystals closer together and produces a fairly sharp 10 Å peak. The disorder produced by Ca^{++} exposes more surface for adsorption. The apparent water vapor surface area is also affected by hydration of the Ca^{++} ion. Slabaugh (42, p. 436-437) has shown the same differences in water vapor adsorption by homoionic bentonites with monovalent and divalent cations on the exchange sites.

The Porosity of Terrigenous Marine Sediments. Data from 110 nitrogen desorption isotherms of sediments from the area shown in Figure 8 exhibit an insignificant amount of pore volume for pores of radius above 50 Å. From 50 Å down, the pore volume per increment of pore radius increases to a peak value in the range of 18 to 24 Å (Figure 14). The pore volume then decreases below this point. The pore size distributions show that, if the material is porous, nearly all of the pores are smaller than 50 Å in radius. It should be pointed out that these marine sediments may not be porous at all in the sense of rigid pores that do not expand or contract with gas pressure. Instead the hysteresis and the sharp dip in the desorption isotherm between P/P_o of 0.4 and 0.6 can be caused by expansion (separation) of the clay mineral

FIGURE 14

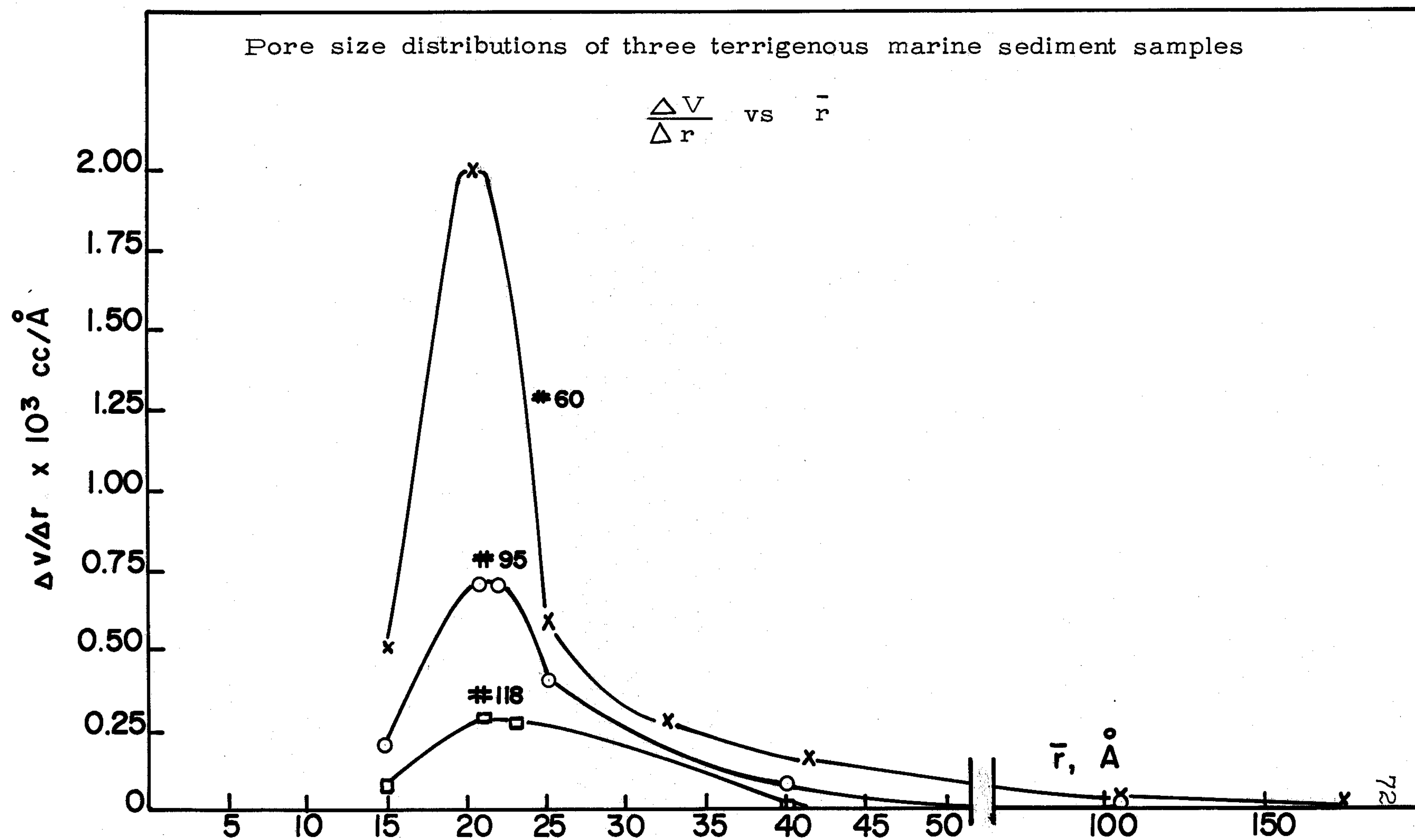
Pore size distributions of three terrigenous marine sediment samples
$\frac{\Delta V}{\Delta r}$ vs $\bar{r}$
$\Delta v/\Delta r \times 10^3$ cc/Å
2.00
1.75
1.50
1.25
1.00
0.75
0.50
0.25
0
5
10
15
20
25
30
35
40
45
50
100
150
$\bar{r}$, Å
#60
#95
#118

platelets allowing some penetration of the nitrogen molecule (Figure 10). The same form of hysteresis is produced with "pure" montmorillonite (Figure 15) but kaolinite, illite and chlorite do not show it. The mechanical model described by Hirst (see p. 27)(26, p. 22-28) can explain the adsorption-desorption hysteresis in montmorillonite type clay minerals. The smaller the base exchange capacity of the clay mineral the smaller the forces holding the crystals together. If this binding force is weak enough then the pressure of the nitrogen could cause some separation of the crystals. After adsorption has taken place between the crystal surfaces they act similar to pores and require a lower pressure to desorb, resulting in the adsorption-desorption hysteresis demonstrated by both montmorillonite and terrigenous marine sediments.

A second explanation, one that has more experimental evidence, is based on degraded interlayer material held between the clay mineral crystals. Chlorite is a series of 2:1 clay mineral crystals with a layer of gibbsite ($Al_4(OH)_{12}$), brucite ($Mg_6(OH)_{12}$), or hydrated iron oxide between the crystals as shown in Figure 16. If through chemical and physical processes some of the interlayered material is removed, but not enough to allow the crystals to collapse

FIGURE 15

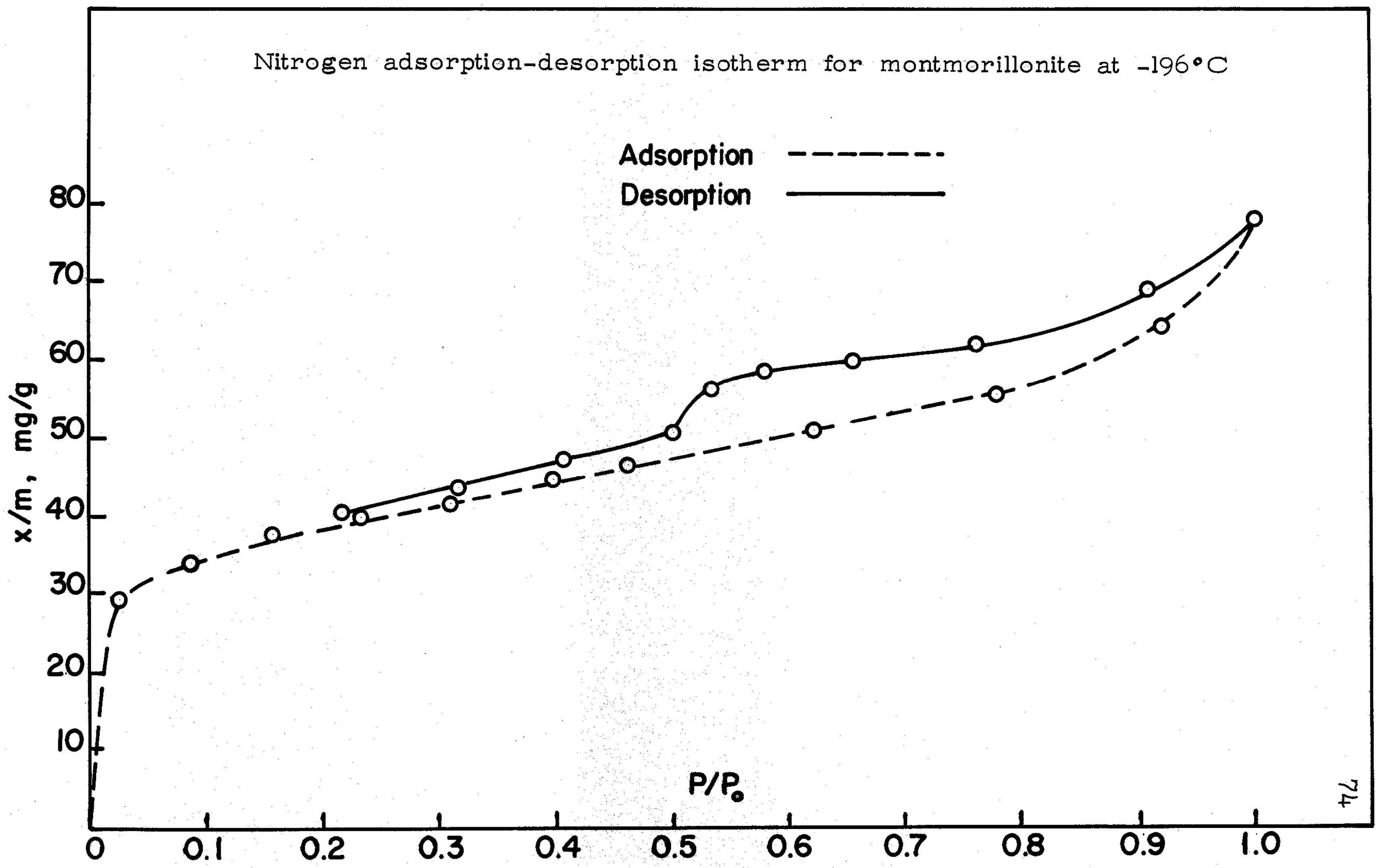

Nitrogen adsorption-desorption isotherm for montmorillonite at -196°C

FIGURE 16

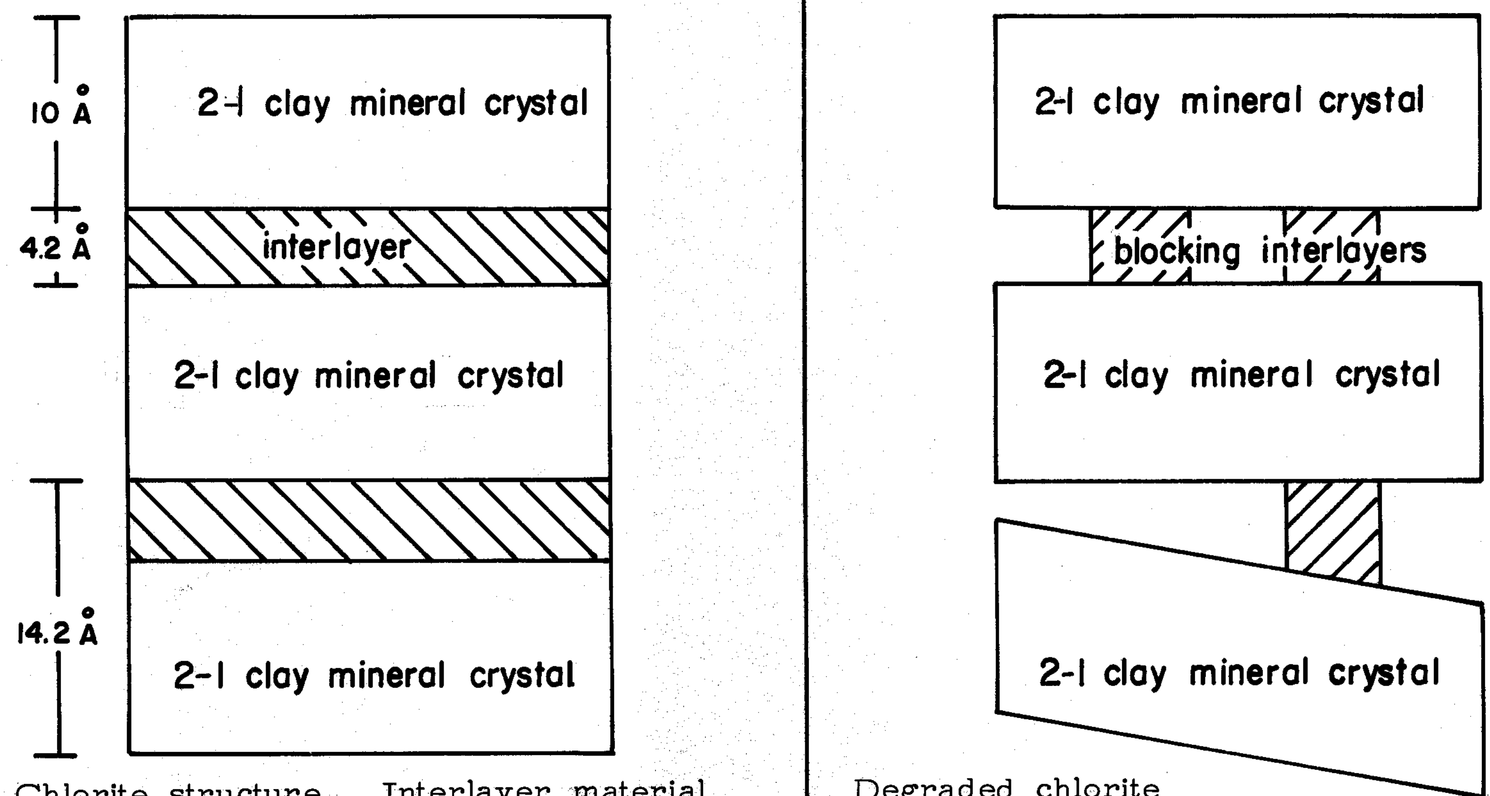

Chlorite structure. Interlayer material brucite, gibbsite or hydrated iron oxide

Degraded chlorite structure or Interlayered montmorillonite structure

Structure models of chlorite and degraded chlorite or interlayered montmorillonite completely, the result would be a labyrinth of small pores as shown in Figure 16. X-Ray diffraction patterns on marine sediments show degraded chlorite patterns which become more pronounced in high surface area samples where glauconite pellets predominate. The patterns become more diffuse with less sharp peaks indicating random orientation of the clay mineral crystals. High nitrogen surface area montmorillonites also show similar broad peaks. Barrer and MacLeod (1, p. 1290-1307) have demonstrated the same phenomenon for montmorillonite with tetra-alkyl ammonium ions on the exchange sites. As shown in Figure 17, $N(CH_3)_4^+$-montmorillonite shows greater nitrogen adsorption than $N(C_2H_5)_4^{+4}$-montmorillonite and a higher surface area. The difference in adsorption is explained in this case by the difference in the volume of space between the plates filled by the C_2H_5 group compared to the CH_3 group.

Further evidence of only small pores existing in marine sediments is illustrated in Figure 18. When a material contains very small pores whose walls make a substantial contribution to the total surface, these pores will be filled by capillary condensation at a low pressure where the n value is low. Filling of these pores reduces the surface available for

FIGURE 17

Nitrogen adsorption-desorption isotherms of tetra-alkyl ammonium montmorillonites

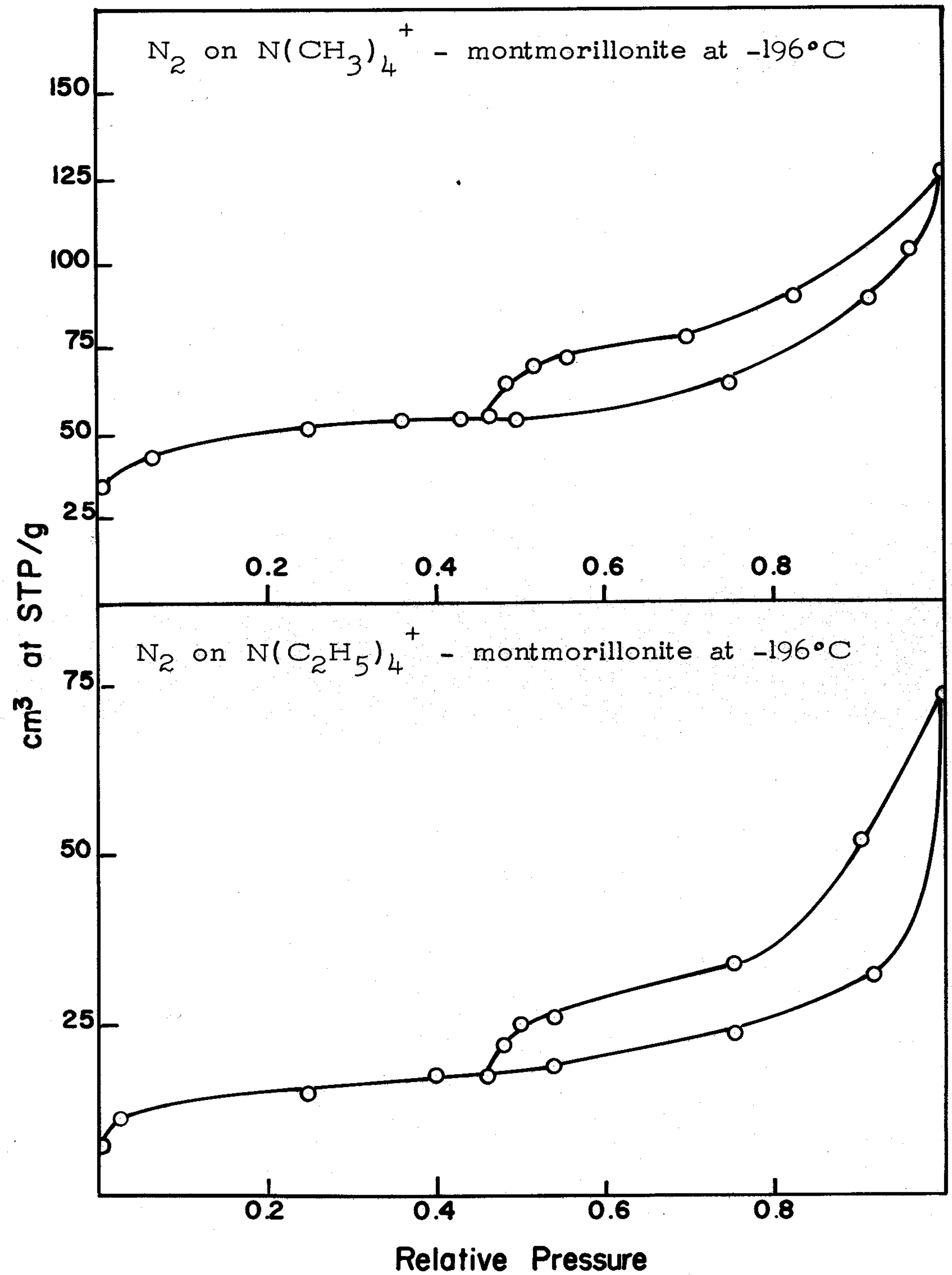

FIGURE 18

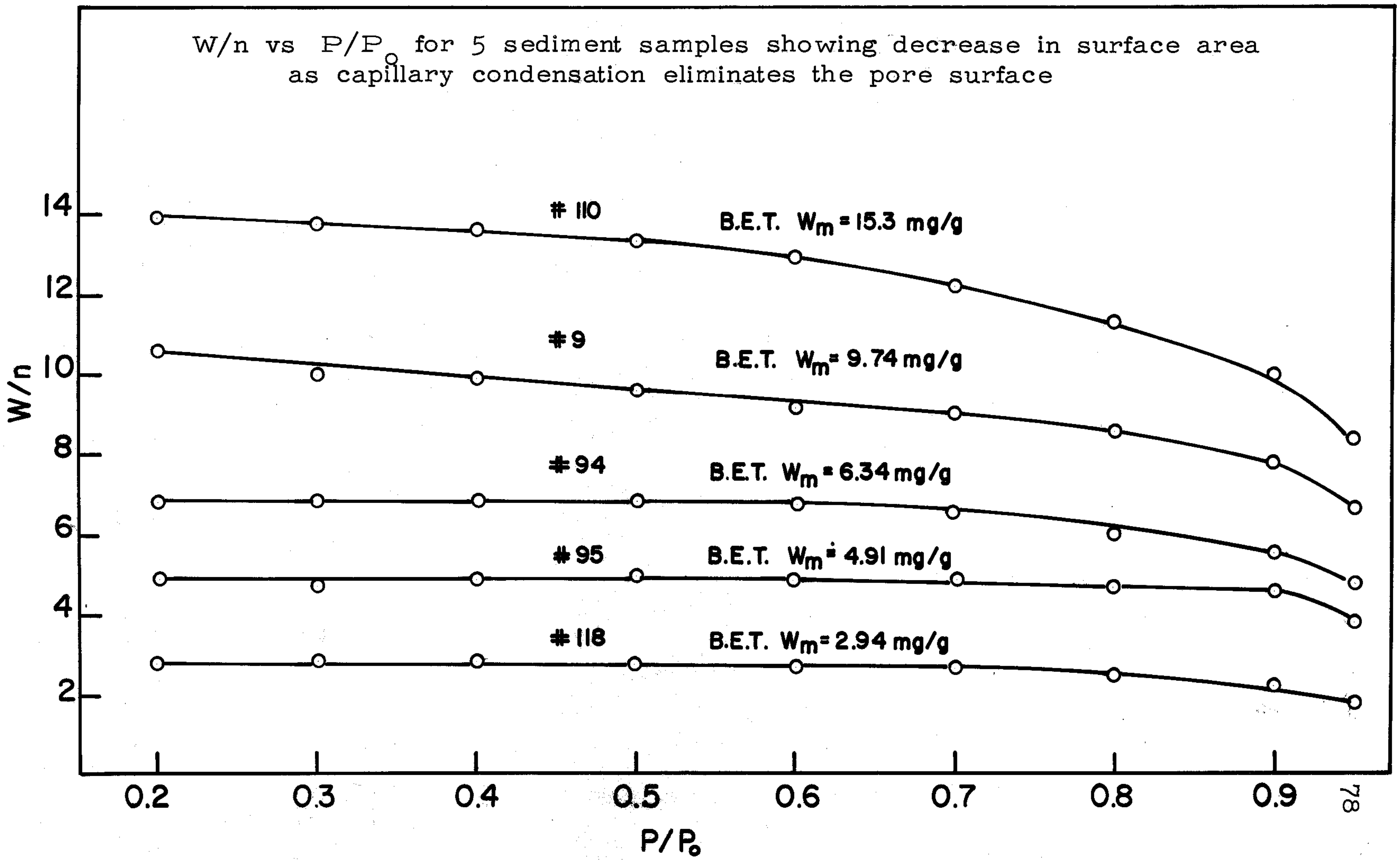
W/n vs P/P$_o$ for 5 sediment samples showing decrease in surface area as capillary condensation eliminates the pore surface
110
B.E.T. W_m = 15.3 mg/g
9
B.E.T. W_m = 9.74 mg/g
94
B.E.T. W_m = 6.34 mg/g
95
B.E.T. W_m = 4.91 mg/g
118
B.E.T. W_m = 2.94 mg/g
W/n
14
12
10
8
6
4
2
0.2
0.3
0.4
0.5
0.6
0.7
0.8
0.9
P/P$_o$

further multilayer adsorption. Further, they contribute very little to the total W value. Therefore, if W/n is plotted vs P/P_o the W/n value will decrease as P/P_o increases as shown in Figure 18. The reverse will be the case for a material containing relatively large pores because capillary condensation is then a large contributor to the total W value and is more pronounced at higher P/P_o values. Calculations of the total pore surface, $\sum A_p$ in Appendix 3, shows that the walls of pores with a radius greater than 20 Å contribute only about 50% of the total surface for the terrigenous marine sediments samples measured in this investigation. The adsorption-desorption isotherms do not quite meet at P/P_o of 0.4. Instead, the desorption isotherm remains slightly above the adsorption isotherm which also indicates the existence of pores with radius less than 20 Å.

An interesting consideration on the porosity of terrigenous marine sediments is the fact that according to the Frenkel-Halsey-Hill equation a free surface material with the same B.E.T. surface as the sediments investigated will adsorb more nitrogen by multilayer adsorption than these sediments will adsorb by both multilayer adsorption and capillary condensation. This results from the reduction of surface by condensation into the small pores of the sediments, while a free surface material will maintain the same total surface throughout the complete range of P/P_o values available for multilayer adsorption.

Clay Minerals in Terrigenous Marine Sediments. Figure 19 shows the diffractograms of eight terrigenous marine sediment samples from the area in Figure 8. The samples range from No. 118 twelve miles off shore to No. 110 thirty four miles off shore. The most important general feature that is noted in the diffractograms is the scarcity and broadness of peaks obtained in samples No. 60 and 110 compared to samples taken nearer shore. The composition of samples No. 60 and 110 show very little evidence of silica but all of the samples from nearer to shore show strong quartz and other silica peaks (Table 11). Samples 60 and 110 show no evidence of kaolinite, true 2:2 chlorite, nor the behavior of the expanding montmorillonite class, all of which are evident in the other six samples analysed. The 17-18 Å peak after Ca^{++} saturation and solvation, characteristic of the expanding montmorillonite class, are strong in all samples except No. 60 and 110. The 10 Å non-expanding peak is stronger the nearer shore the sample

TABLE XI

Clay minerals and silica identified by x-ray diffraction in samples No. 118, 95, 26, 94, 6, 13, 60, 110 of terrigenous marine sediment.

Sample No.	Miles from shore	
118	12	(1) Silica (2) Kaolinite (3) Expanding montmorillonite class (4) Chlorite (5) Illite and/or glauconite and/or mica
95	19	(1) Silica (2) Kaolinite (3) Expanding montmorillonite class (4) Chlorite (5) Illite and/or glauconite and/or mica
26	19	(1) Silica (2) Kaolinite (3) Expanding montmorillonite class (4) Chlorite (5) Illite and/or glauconite and/or mica
94	22	(1) Silica (2) Kaolinite (3) Expanding montmorillonite class (4) Chlorite (5) Illite and/or glauconite and/or mica
6	24	(1) Silica (2) Kaolinite (small) (3) Expanding montmorillonite class (large) (4) Chlorite (small) (5) Illite and/or glauconite and/or mica (small)

TABLE XI Continued

Sample No.	Miles from shore	
13	27	(1) Silica (2) Kaolinite (3) Expanding montmorillonite class (4) Chlorite (5) Illite and/or glauconite and/or mica
60	33	(1) Silica (small) (2) No definite expansion peak, but after heating and/or K^+ saturation, and heating there is a strong 10 Å peak, evidence of mixed layered glauconite or disordered illite. Color indicates mixed layered glauconite. (3) Illite and/or glauconite and/or mica (small)
110	34	(1) No evidence of silica (2) No evidence of kaolinite (3) No solvation expansion peak but heat and/or K^+ saturation and heat produces strong 10 Å peak. Evidence of mixed layered glauconite or disordered illite (color indicates glauconite) (4) Illite and/or glauconite and/or mica (small)

FIGURE 19a

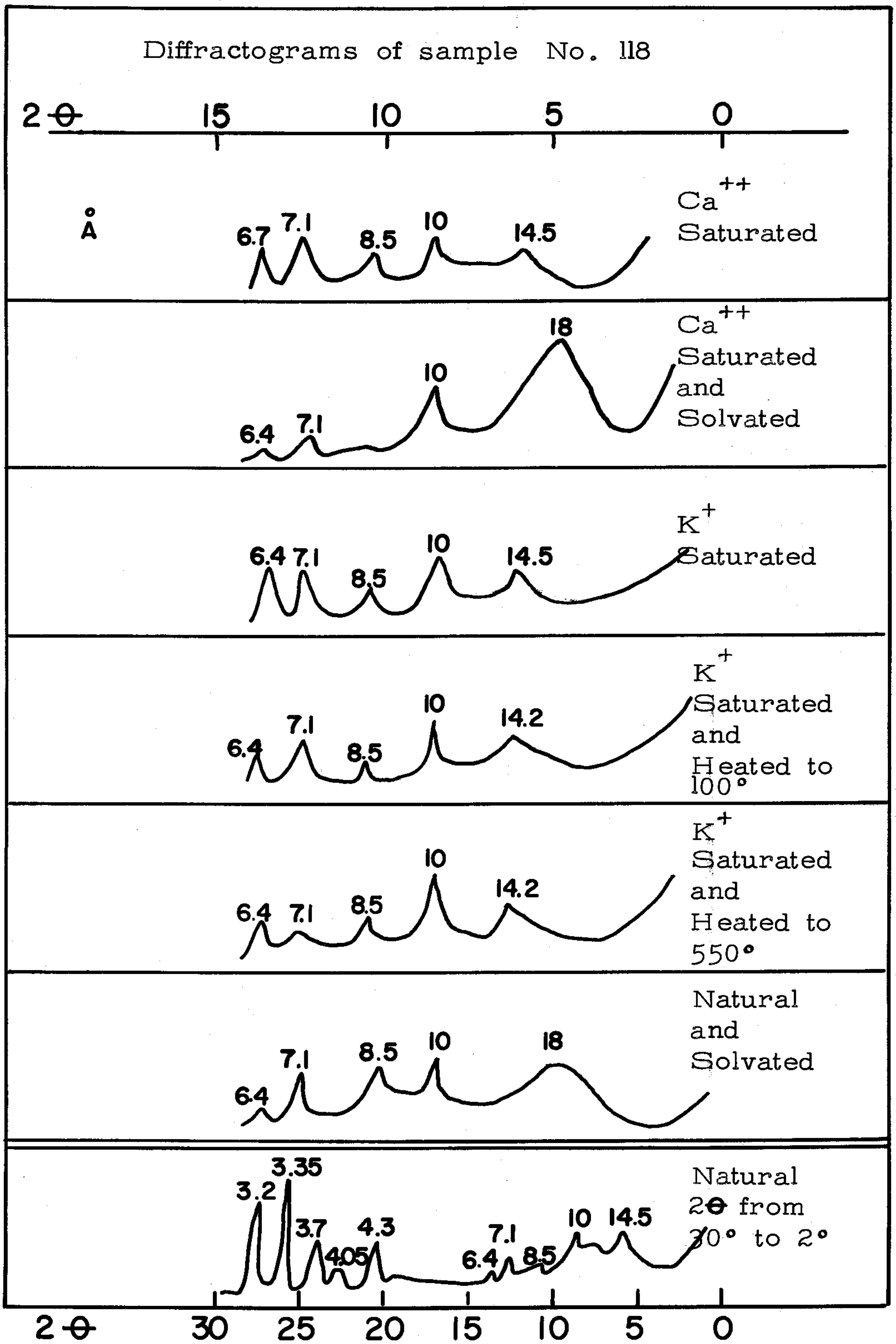
Diffractograms of sample No. 118
2θ
15
10
5
0
Å
6.7 7.1 8.5 10 14.5
Ca++ Saturated
6.4 7.1 10 18
Ca++ Saturated and Solvated
6.4 7.1 8.5 10 14.5
K+ Saturated
6.4 7.1 8.5 10 14.2
K+ Saturated and Heated to 100°
6.4 7.1 8.5 10 14.2
K+ Saturated and Heated to 550°
6.4 7.1 8.5 10 18
Natural and Solvated
3.2 3.35 3.7 4.05 4.3 6.4 7.1 8.5 10 14.5
Natural 2θ from 30° to 2°
2θ
30
25
20
15
10
5
0

FIGURE 19b

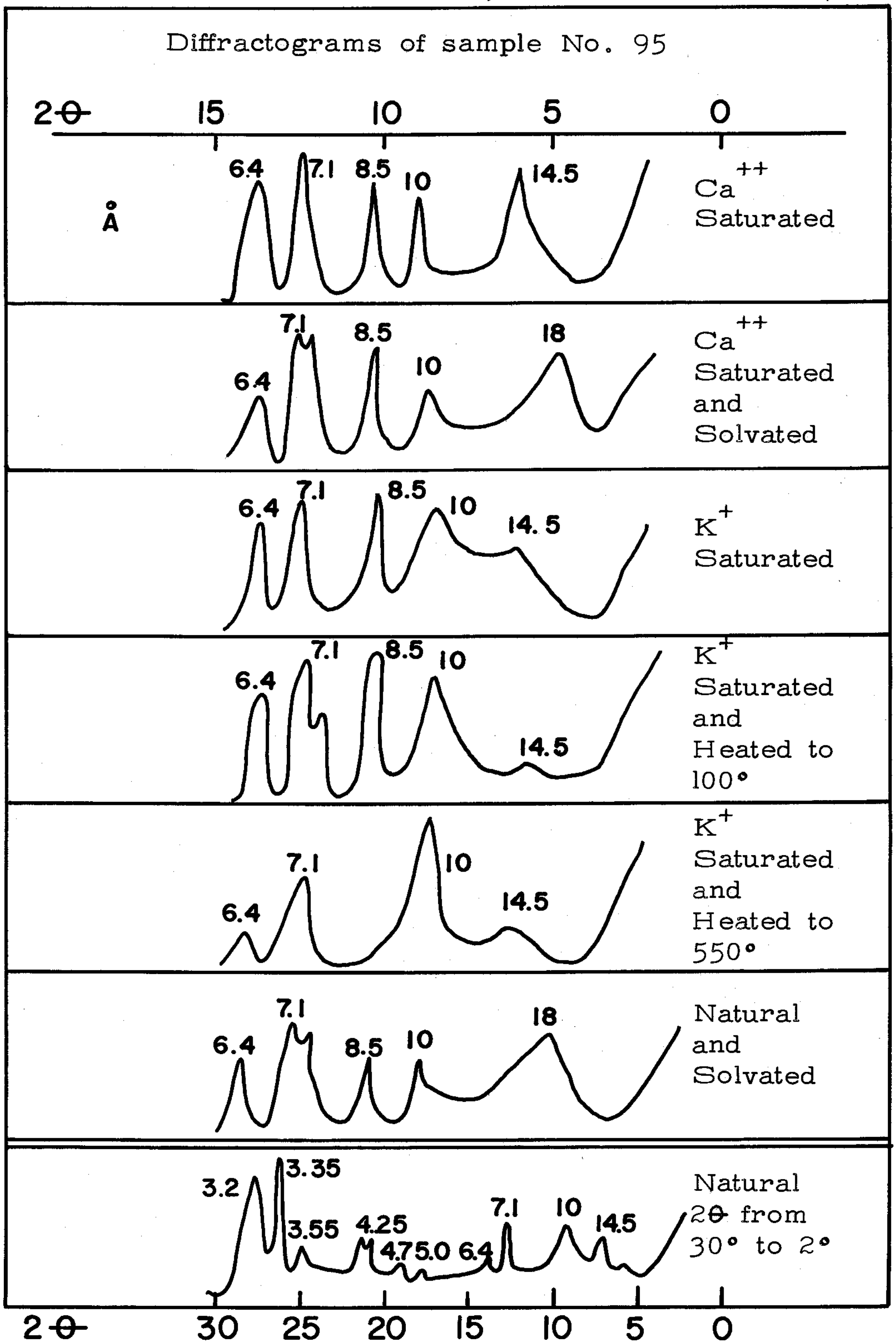
Diffractograms of sample No. 95
2θ
15
10
5
0
Å
6.4
7.1
8.5
10
14.5
Ca++ Saturated
18
Ca++ Saturated and Solvated
K+ Saturated
K+ Saturated and Heated to 100°
K+ Saturated and Heated to 550°
Natural and Solvated
3.2
3.35
3.55
4.25
4.75
5.0
Natural 2θ from 30° to 2°
30
25
20

FIGURE 19c

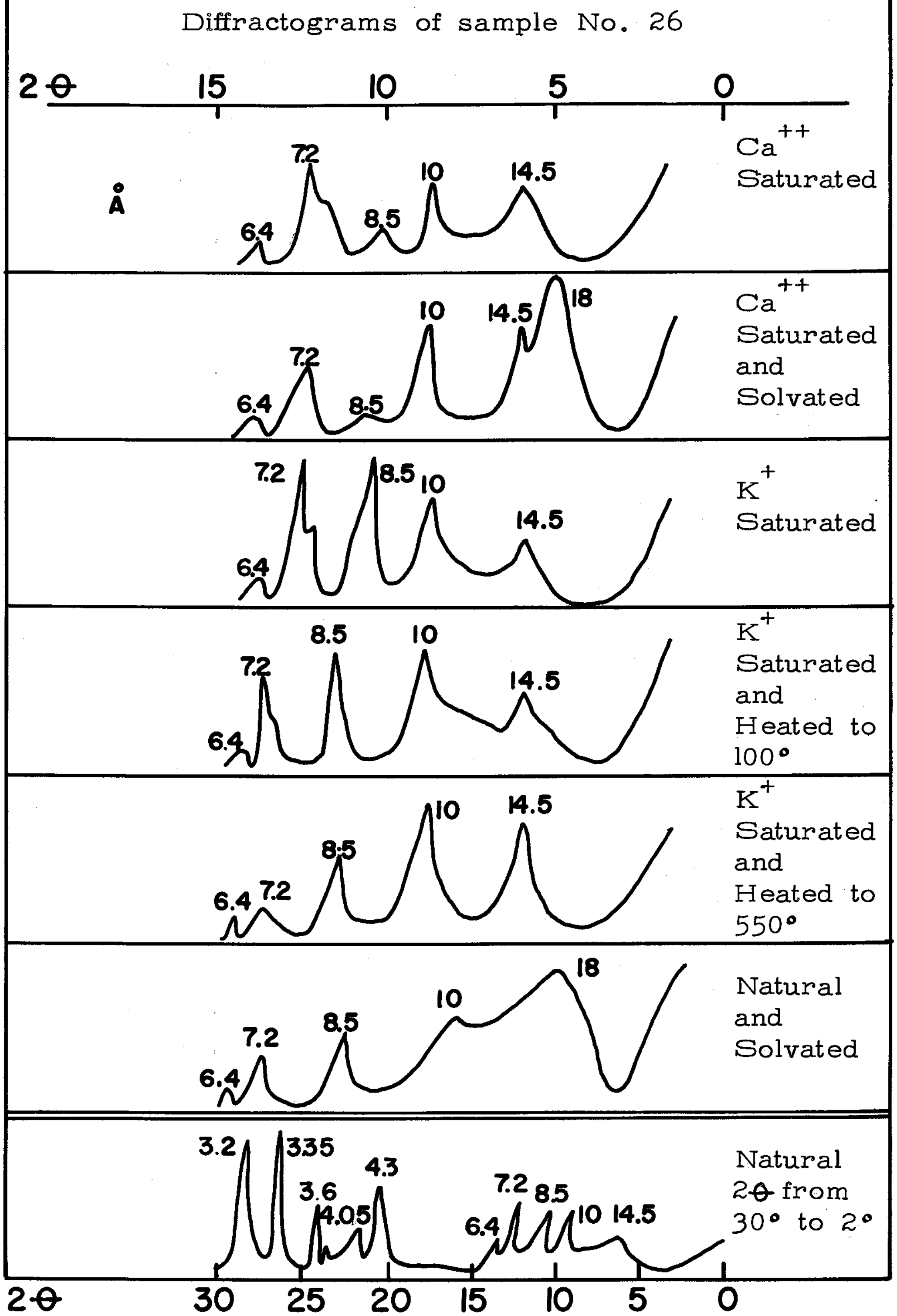
Diffractograms of sample No. 26
2θ
15
10
5
0
Å
7.2
10
14.5
6.4
8.5
Ca++ Saturated
10
14.5
18
7.2
6.4
8.5
Ca++ Saturated and Solvated
7.2
8.5
10
14.5
6.4
K+ Saturated
8.5
10
7.2
14.5
6.4
K+ Saturated and Heated to 100°
10
14.5
8.5
6.4
7.2
K+ Saturated and Heated to 550°
18
10
8.5
7.2
6.4
Natural and Solvated
3.2
3.35
4.3
3.6
4.05
7.2
8.5
10
14.5
6.4
Natural 2θ from 30° to 2°
2θ
30
25
20
15
10
5
0

FIGURE 19d

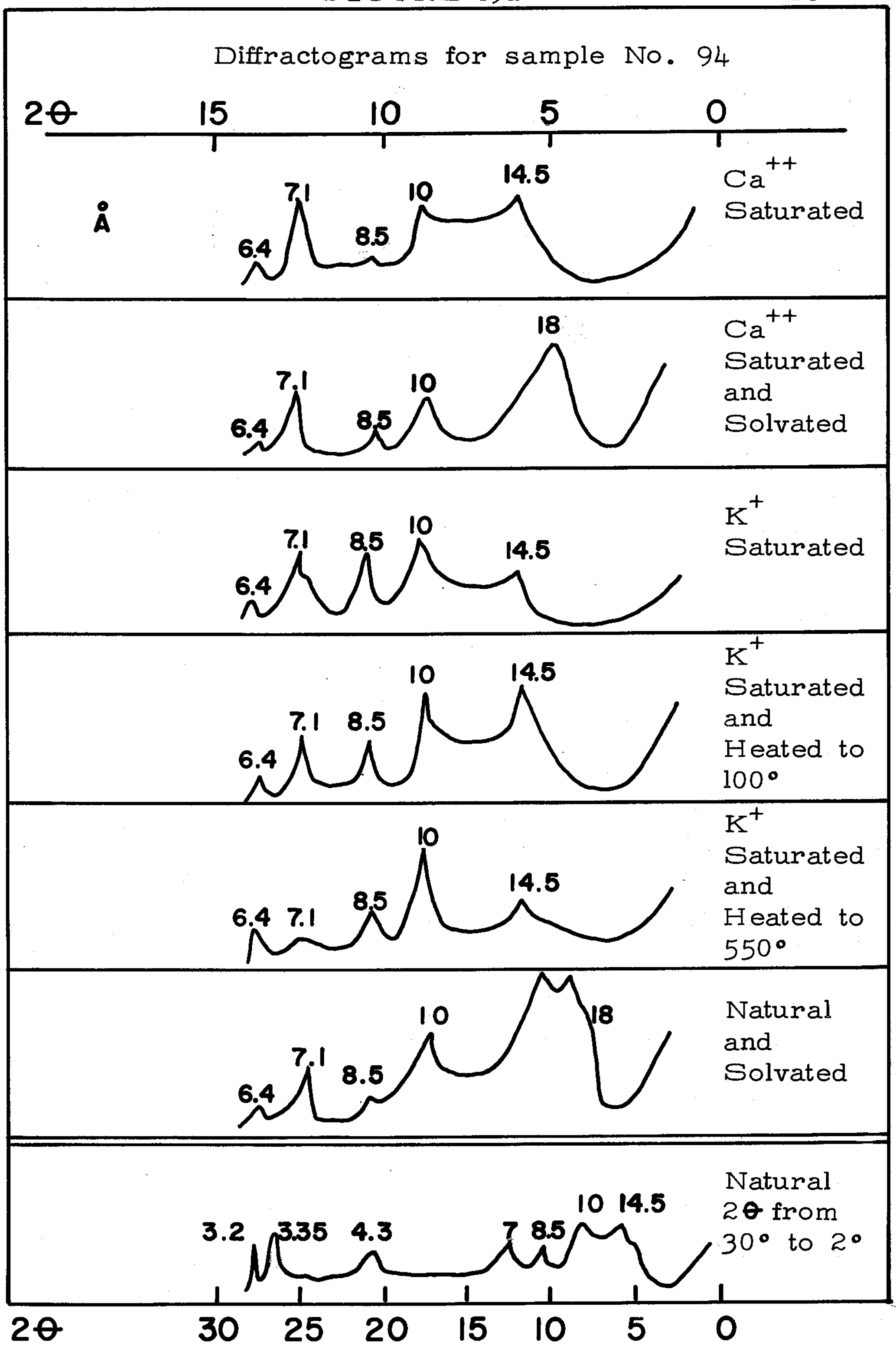

Diffractograms for sample No. 94
2θ
15
10
5
0
Å
Ca++ Saturated
6.4
7.1
8.5
10
14.5
Ca++ Saturated and Solvated
6.4
7.1
8.5
10
18
K+ Saturated
6.4
7.1
8.5
10
14.5
K+ Saturated and Heated to 100°
6.4
7.1
8.5
10
14.5
K+ Saturated and Heated to 550°
6.4
7.1
8.5
10
14.5
Natural and Solvated
6.4
7.1
8.5
10
18
Natural 2θ from 30° to 2°
3.2
3.35
4.3
7
8.5
10
14.5
2θ
30
25
20
15
10
5
0

FIGURE 19e

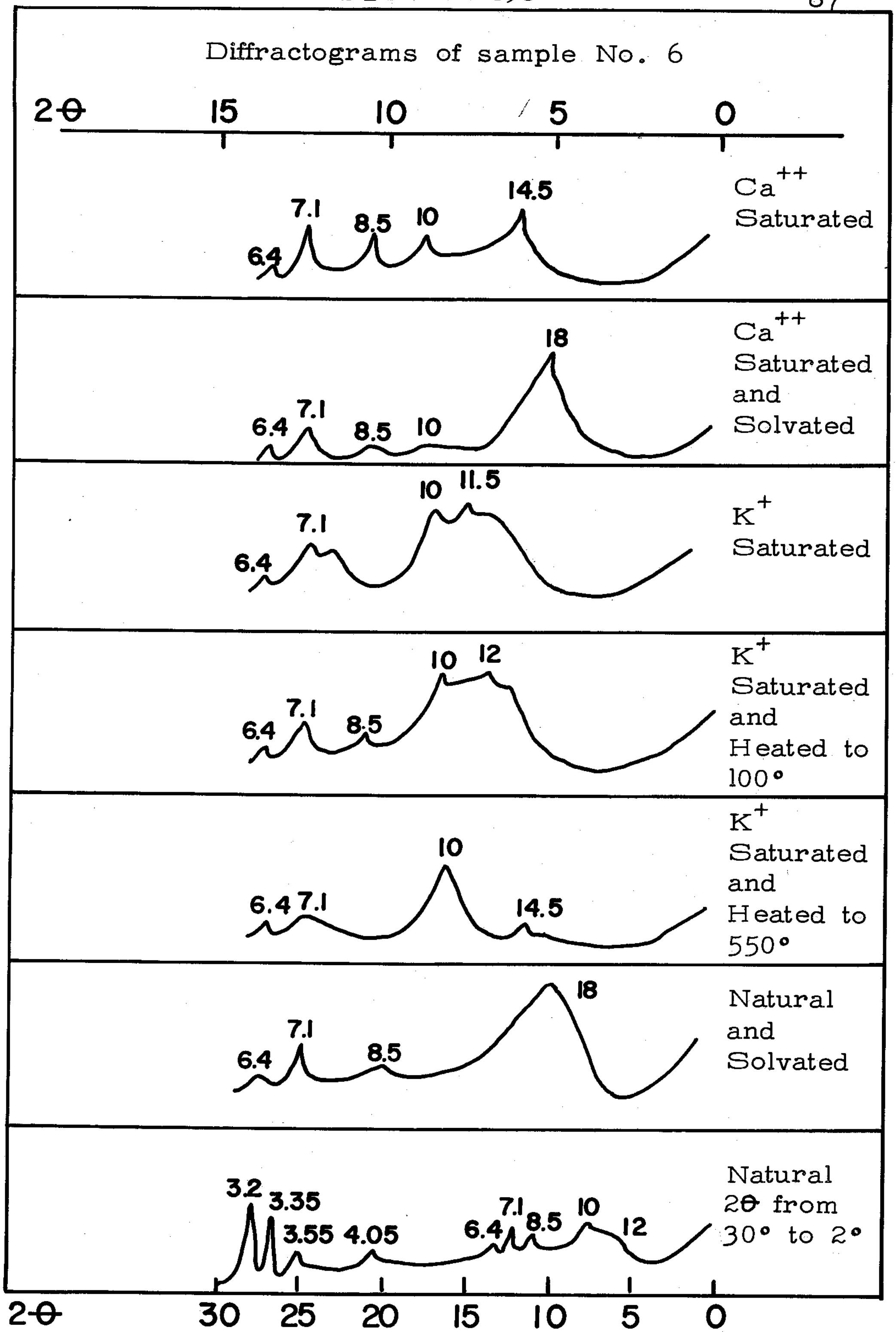
Diffractograms of sample No. 6
2-θ
15
10
5
0
14.5
7.1
8.5
10
6.4
Ca++ Saturated
18
6.4
7.1
8.5
10
Ca++ Saturated and Solvated
10
11.5
7.1
6.4
K+ Saturated
10
12
7.1
6.4
8.5
K+ Saturated and Heated to 100°
10
6.4
7.1
14.5
K+ Saturated and Heated to 550°
18
7.1
6.4
8.5
Natural and Solvated
3.2
3.35
3.55
4.05
6.4
7.1
8.5
10
12
Natural 2θ from 30° to 2°
2-θ
30
25
20
15
10
5
0

FIGURE 19f

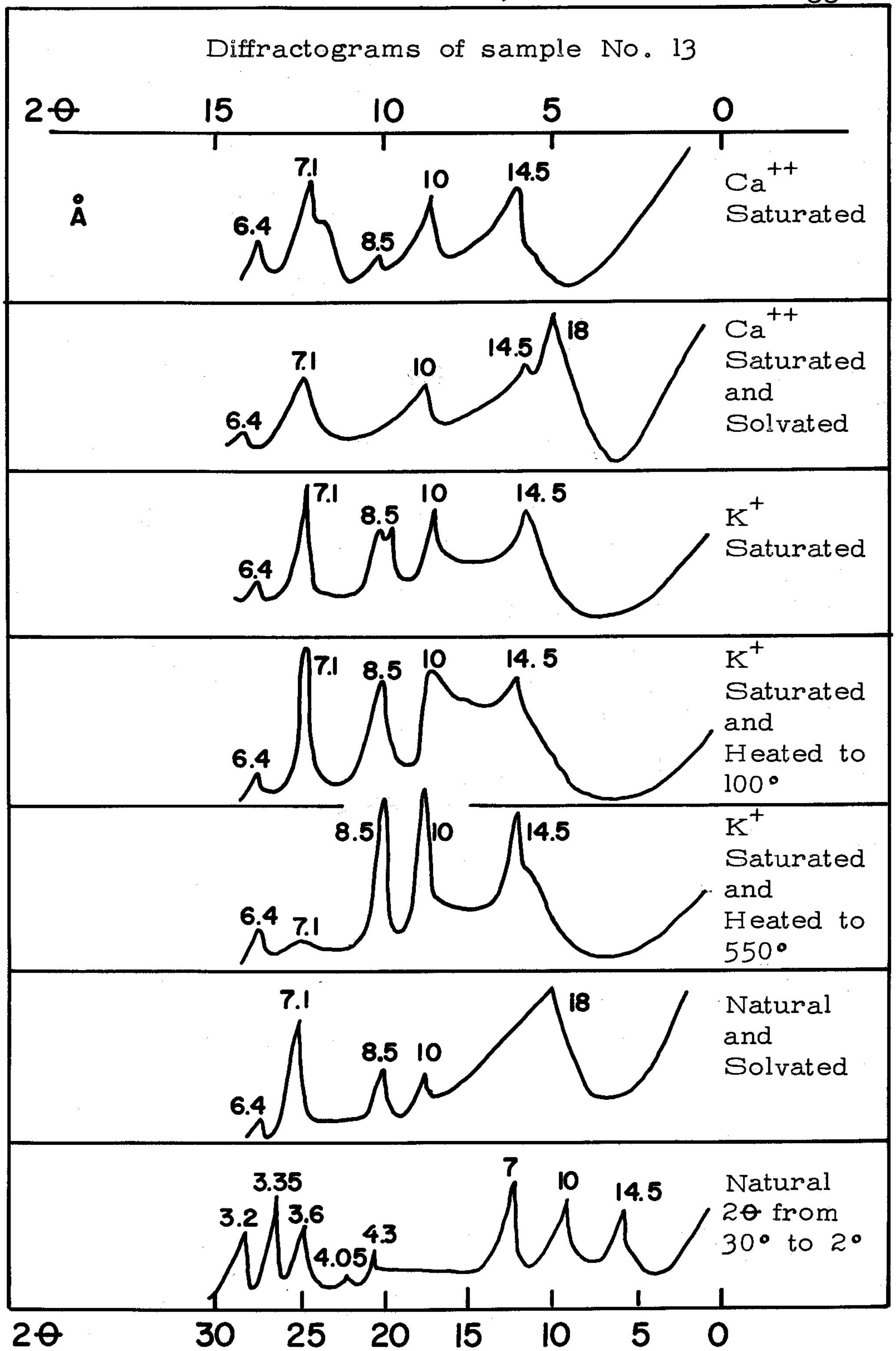
Diffractograms of sample No. 13
2θ
15
10
5
0
Å
6.4
7.1
8.5
10
14.5
Ca++ Saturated
6.4
7.1
10
14.5
18
Ca++ Saturated and Solvated
6.4
7.1
8.5
10
14.5
K+ Saturated
6.4
7.1
8.5
10
14.5
K+ Saturated and Heated to 100°
6.4
7.1
8.5
10
14.5
K+ Saturated and Heated to 550°
6.4
7.1
8.5
10
18
Natural and Solvated
3.2
3.35
3.6
4.05
4.3
7
10
14.5
Natural 2θ from 30° to 2°
2θ
30
25
20
15
10
5
0

FIGURE 19g

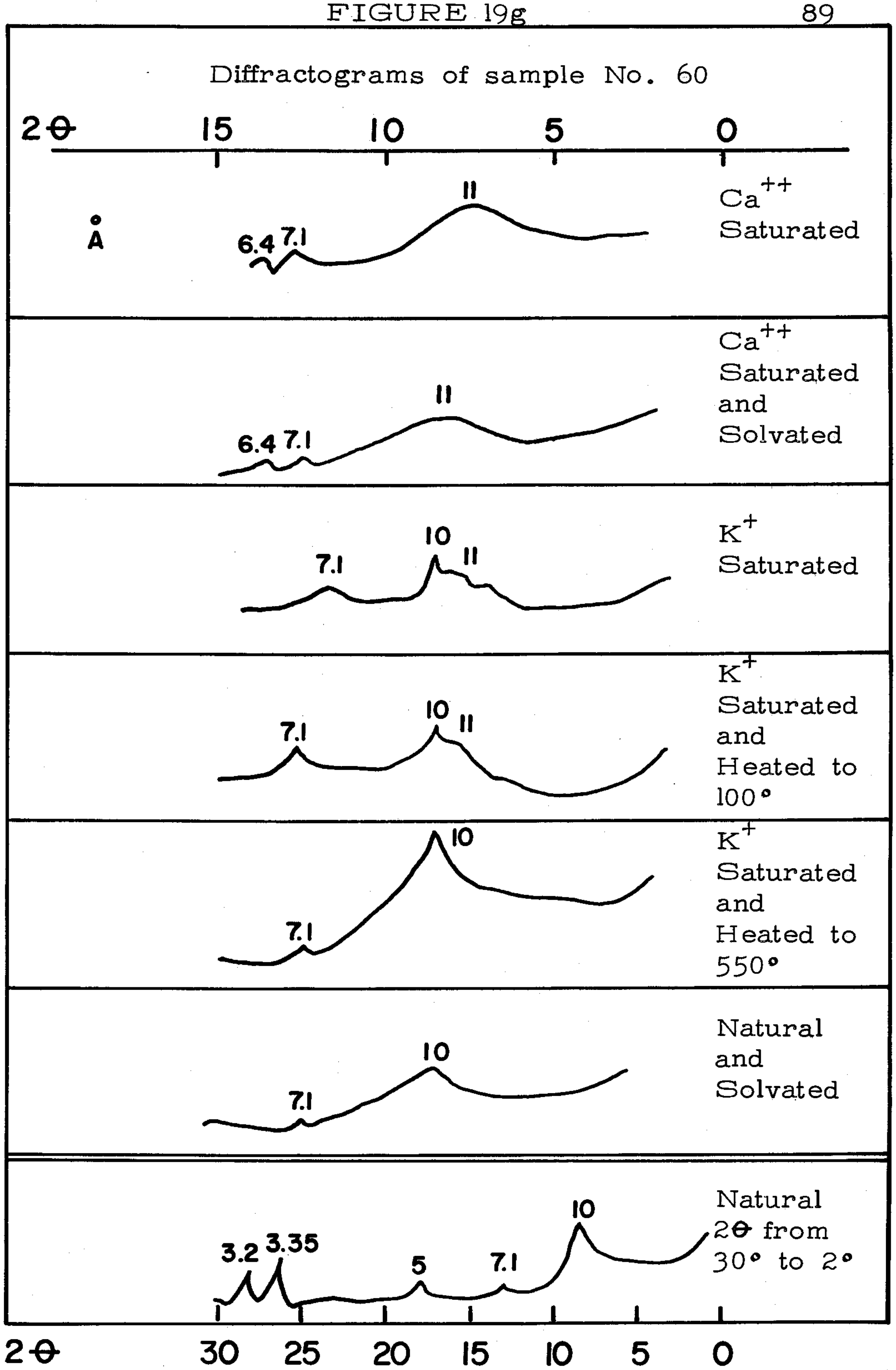
Diffractograms of sample No. 60
2θ
15
10
5
0
Å
6.4 7.1
11
Ca++ Saturated
6.4 7.1
11
Ca++ Saturated and Solvated
7.1
10
11
K+ Saturated
7.1
10
11
K+ Saturated and Heated to 100°
10
7.1
K+ Saturated and Heated to 550°
10
7.1
Natural and Solvated
3.2 3.35
5
7.1
10
Natural 2θ from 30° to 2°
2θ
30
25
20
15
10
5
0

FIGURE 19h

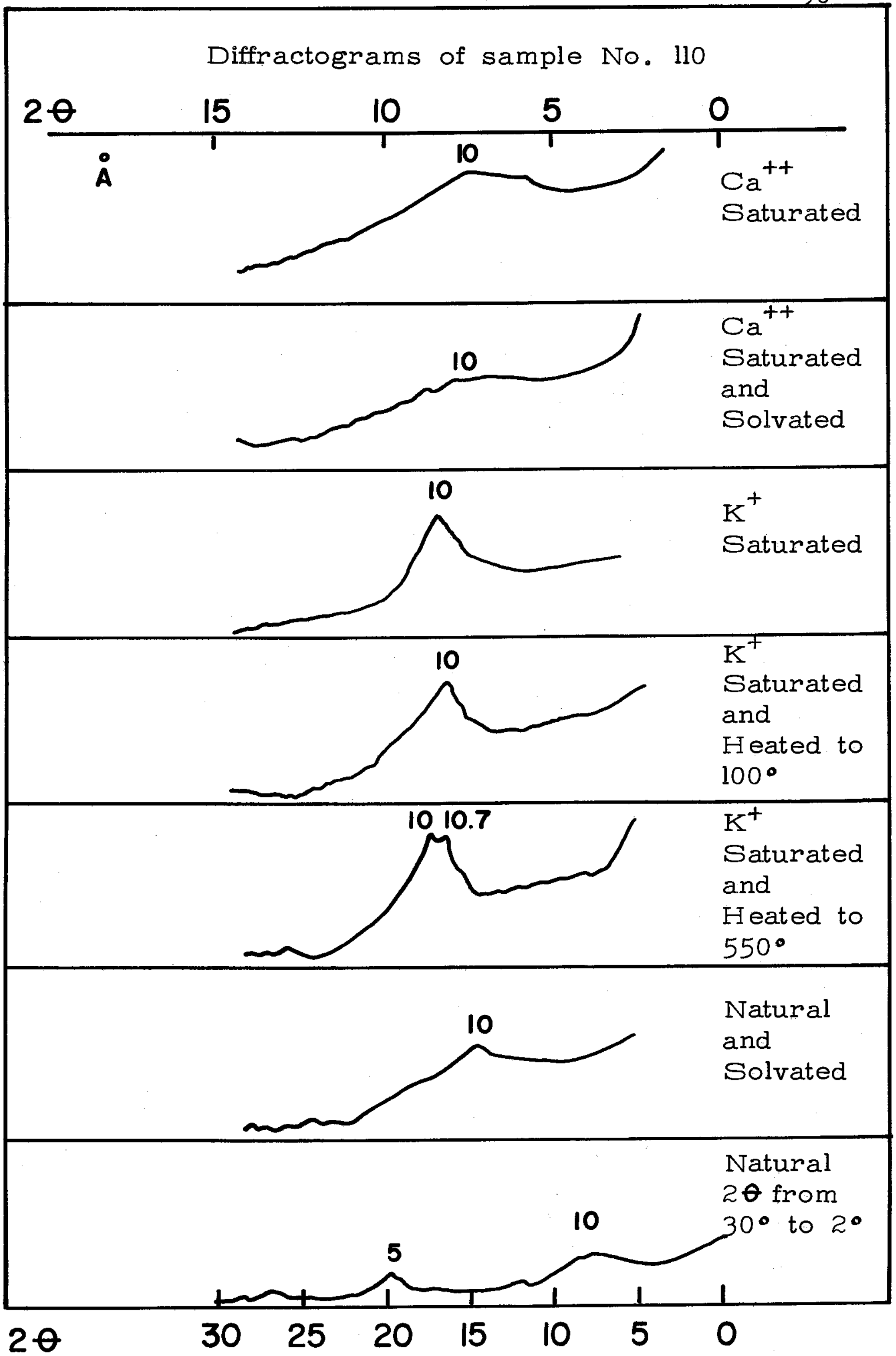
Diffractograms of sample No. 110
2θ
15
10
5
0
Å
10
Ca++ Saturated
10
Ca++ Saturated and Solvated
10
K+ Saturated
10
K+ Saturated and Heated to 100°
10 10.7
K+ Saturated and Heated to 550°
10
Natural and Solvated
Natural 2θ from 30° to 2°
10
5
2θ
30
25
20
15
10
5
0

was taken. The 14.5 Å 2:2 chlorite mineral peak is stronger nearer shore. There is very little evidence of this peak in samples 60 and 110.

Comparison of the diffractograms of samples No. 60 and 110 in Figure 20 with the diffractograms given by Burst for the ferriferous clay minerals (the glauconites) shown in Figure 5 indicate that these two samples are predominately interlayered or disordered glauconite clay minerals. The green color of these two samples indicates the presence of iron and places them in the glauconite class instead of the illite class (Figure 4). The diffractograms of the other six samples shown in Figure 19 indicate them to be composed of mixtures of montmorillonite, chlorite, illite, glauconite, kaolinite and silica as shown in Table 11. Sample No. 6 has an exceptionally high percentage of montmorillonite and also has a high surface area (Table 9). The color is light tan with a hint of green. This sample is an anomaly according to data shown in Table 5. The surface area compares with those given for green glauconitic samples No. 60 and 110. Diffractograms of sample No. 6 show strong 18 Å expansion peaks after Ca^{++} saturation and solvation but K^{+} saturation produces a broad peak from 10 to 14.5 Å. The diffractograms and adsorption measurements indicate that this sample is chiefly montmorillonite with interlayered material interspersed between some of the clay crystals. The color indicates there is less iron in sample 6 than in samples 110 and 60. Sample No. 6 could be classed as degraded or mixed layered illite.

Suggested Further Investigations

There is yet further work to be done by the techniques used in this investigation and by other techniques that would further the understanding of the structure of marine sediments as well as the chemical processes taking place at their liquid solid interface.

Several projects suggested by this investigation are listed below:

1. Separation and analysis of the various clay minerals composing the sediments would be helpful. Quantitative data cannot be obtained by any other means.

2. Measurement of the base exchange capacity of the sediments would be helpful in understanding the structure and the cation exchanges taking place on the sediments.

3. Quantitative measurement of the different ionic species bonded on the exchange sites of the clay minerals

would be very beneficial in understanding both the chemistry and structure of the sediments.

4. More work could be done on the study of the organic composition of sediments, including an investigation of adsorption of organic compounds on the sediments as well as amines bonded to the exchange sites of the clay minerals.

5. Measurement of the redox condition of the sediments would aid substantially in predicting possible chemical processes. Investigation of the content of nitrogen in the sediments, especially in the form of amines would also aid in understanding the oxidizing or reducing conditions of the sediments.

6. More information could be obtained by applying the techniques used in this investigation on deeper sediments, even on pelagic deposits. Structure studies of this kind in other terrigenous regions for comparison would also be helpful.

7. Study of the effect of saturating the exchange sites with other cations such as Mg^{++}, Fe^{++}, Fe^{+++}, Al^{+++}, H^{+}, NH_4^{+} and amines on the sediments would be of value in defining the formation of the clay minerals found in marine sediments.

8. Chemical analysis of the sediments off the Oregon

coast has never been made. Chemical analysis performed in the same manner as Goldberg and Arrhenius (19, p. 153-212) and El Wakeel and Riley (14, p. 110-146) would help to define the chemical structure of these sediments. These analyses of the Oregon coast sediments could be compared with the analysis of marine sediments in other regions.

9. Investigation of the adsorption properties of ammonia and carbon dioxide would also help understand the chemical processes in the sediments.

10. Study of adsorption of hydrocarbons by the sediments out of water solution could throw some light on the production of petroleum.

SUMMARY AND CONCLUSIONS

The adsorption characteristics and x-ray patterns of the terrigenous marine sediments analyzed in this investigation show a definite change in the structure of the silicate minerals as the depth and distance from shore is increased.

The clay minerals in glauconite pellets are very disordered especially beyond a depth of 200 fathoms. The x-ray patterns change from well defined peaks to broad diffuse peaks at this point. The surface areas and pore volumes also increase markedly. Both factors indicate disorder in the clay minerals. The composition of the sediments in shallower depths, closer to shore, are similar in composition to the land mass of the vicinity. It would be very difficult if not impossible to compare the deeper samples with any terrigenous source and it must be concluded that some form of change has taken place within the marine environment to produce their structure.

There are two possible mechanisms by which these disordered clay minerals can be formed:

(1) Expanding montmorillonite clay minerals depositing along with silica, gibbsite, brucite, and iron oxide under the pressure of the sea water at these depths may be expanded

enough to allow interlayer deposits to form as shown in Figure 16. These deposits will then disrupt the order of stacking of the clay crystals, causing the disordered x-ray peaks, the increase in surface areas and the large pore volumes. Interlayer deposits can be grown synthetically in montmorillonite (9).

(2) The 2:2 nonexpanding chlorite when exposed to marine environment, where there are all kinds of chemical species and mechanical forces foreign to land environment, could have much of its interlayered material removed. This could be effected by either chemical processes, solution, or mechanical actions of the water. The final product would be the same by either mechanism. Both types of clay minerals can be detected by x-ray where the disordering process has not proceeded far enough to make the diffractograms too diffused to read.

As outlined in this discussion, gas adsorption techniques used jointly with x-ray diffraction, ferromagnetic separation and particle size analysis are valuable tools to help define the structure and characteristics of marine sediments. Modifications suggested for using W/n values and only one pressure reading would simplify the whole procedure. This investigation shows that it is only necessary, in the case of terrigenous sediments, to measure the surface area in order to know the pore volume because in all cases one was directly related to the other. For comparative gas adsorption surface area measurements it is not necessary to extract any material from the basic silicate minerals of terrigenous marine sediments. The surface areas of extracted samples were directly related to the surface areas measured on unextracted samples. However, it is important not to heat the sample above 80°C. Heating above this temperature will decrease the surface area.

This investigation into the microstructure and surface chemistry of marine sediments is not intended to be exhaustive. Many more phenomena must be investigated. For this reason the final section includes some further projects that would be helpful to further understand the structure and chemistry of marine sediments.

BIBLIOGRAPHY

1. Barrer, R.M. and D.M. MacLeod. Activation of montmorillonite by ion exchange and sorption complexes of tetra-akyl ammonium montmorillonite. Faraday Society Transactions 51:1290-1307. 1955.

2. Barret, Elliot P., Leslie G. Joyner and Paul P. Halenda. The determination of pore volume and area distributions in porous substances. I. Computations from nitrogen isotherms. Journal of the American Chemical Society 73:373-380. 1951.

3. Brunauer, Stephen, P.H. Emmett and Edward Teller. Adsorption of gases in multimolecular layers. Journal of the American Chemical Society 60:309-319. 1938.

4. Burst, J.F. Mineral heterogeneity in glauconite pellets. American Mineralogist 43:481-497. 1958.

5. Burst, John F. "Glauconite Pellets": Their mineral nature and applications to stratigraphic interpretations. American Association of Petroleum Geologists Bulletin 42:310-325. 1958.

6. Bushnell, D. Unpublished research on marine sediments off the coast of Oregon. Corvallis, Oregon. Oceanography Department, Oregon State University. 1962.

7. Byrne, John V. Geomorphology of the continental terrace off the central coast of Oregon. The Ore Bin 24:65-74. 1962.

8. Caroll, Dorothy. Role of clay minerals in the transport of iron. Geochemica et Cosmochemica Acta 14:1-26. 1958.

9. Carstea, D. Unpublished research on synthetically grown interlayered material in montmorillonites. Corvallis, Oregon. Soils Department, Oregon State University. 1963.

10. Cochran, C.N. and L.A. Cosgrove. Pore size distribution of porous Al_2O_3 by mercury porosimeter and

n-butane sorption. Journal of Physical Chemistry 61: 1417-1419. 1957.

11. Cohan, Leonard H. Hysteresis and the capillary theory of adsorption of vapors. Journal of the American Chemical Society 66:90-105. 1944.

12. Coker, R.E. This great and wide sea. Chapel Hill, The University of North Carolina Press, 1954. 325p.

13. Drake, C.L. Pore size distributions in porous materials. Industrial and Engineering Chemistry 41: 780-785. 1949.

14. El Wakeel, S.K. and J.P. Riley. Chemical and mineral studies in deep sea sediments. Geochemica et Cosmochemica Acta 25:110-146. 1961.

15. Emmett, P.H. Multilayer adsorption equations. Journal of the American Chemical Society 68:1784-1789. 1946.

16. Emmett, P.H. and Stephen Brunauer. The use of low temperature van der Waals adsorption isotherms in determining the surface area of iron synthetic catalysts. Journal of the American Chemical Society 59:1553-1564. 1937.

17. Emmett, P.H., Stephen Brunauer and Katherine S. Love. The measurement of surface areas of soils and soil colloids by the use of low temperature van der Waals adsorption isotherms. Soil Science 45:57-65. 1938.

18. Faeth, Paul A. and Charles B. Willingham. Technical bulletin on the assembly, calibration and operation of a gas adsorption apparatus for the measurement of surface area, pore volume distribution, and density of finely divided solids. Pittsburgh, Pennsylvania, Mellon Institute of Industrial Research, 1955. 56p.

19. Goldberg, E.D. and G.O.S. Arrhenius. Chemistry of Pacific pelagic sediments. Geochemica et Cosmochemica Acta 13:153-212. 1958.

20. Grim, Ralph E. Clay mineralogy. New York, McGraw-Hill Book Company Inc, 1953. 348p.

21. Harkins, William D. and George Jura. Surface of solids. X. Extension or the attractive energy of a solid into an adjacent liquid or film, the decrease of energy with distance, and the thickness of films. Journal of the American Chemical Society 66:919-927. 1944.

22. Harkins, William D. and George Jura. Surface of solids. XIII. A vapor adsorption method for the determination of the area of a solid without the assumption of a molecular area, and areas occupied by nitrogen and other molecules on the surface of a solid. Journal of the American Chemical Society 66:1366-1373. 1944.

23. Harkins, William D. and George Jura. An absolute method for the determination of the area of a finely divided crystalline solid. Journal of the American Chemical Society 66:1362-1366. 1944.

24. Harvey, H.W. The chemistry and fertility of sea waters. Cambridge University Press. 1960. 240p.

25. Hendricks, S.B. and C.S. Ross. Chemical composition and genesis of glauconite and celadonite. American Mineralogist 26:683-708. 1941.

26. Hirst, W. The mechanical interaction between mobile insoluble adsorbed films, capillary condensation liquid and fine-structured solids. Faraday Society Discussions 3:22-28. 1948.

27. Huttig, G.R. Zur Auswertung der Adsorption-Isothermen. Monatshefte fur Chemie und Versandte Teile Anderer Wissenchaften 78:177-184. 1948.

28. Jackson, M.L. Soil Chemical Analysis-Advanced Course. Madison, University of Wisconsin, College of Agriculture, Department of Soils. 1956. 991p.

29. Kulp, J. Laurence and Donald R. Carr. Surface area of deep-sea sediments. Journal of Geology 60:148-159. 1952.

30. Laevastu, Taivo. The occurrence of pigments in marine sediments. Journal of Marine Research 17: 325-334. 1958.

31. Langmuir, Irving. Chemical reactions at low pressures. Journal of the American Chemical Society 37:1139-1167. 1915.

32. Livingston, H.K. The cross-sectional areas of molecules adsorbed on solid surfaces. Journal of Colloid Science 4:447-458. 1949.

33. McBain, J.W. and A.M. Bakr. A new sorption balance. Journal of the American Chemical Society 48:690-695. 1926.

34. Orr, Clyde Jr. and J.M. Dallavalle. Fine particle measurement, New York, The Macmillan Co., 1959. 353p.

35. Pauling, Linus. The structure of the micas and related minerals. Proceedings of the National Academy of Science 16:123-129. 1930.

36. Pierce, Conway. Computation of pore sizes from physical adsorption data. Journal of Physical Chemistry 57:149-152. 1953.

37. Pierce, Conway. Effects of interparticle condensation on heats of adsorption and isotherms of powder samples. Journal of Physical Chemistry 63:1076-1079. 1959.

38. Pierce, Conway. The Frenkel-Halsey-Hill equation and capillary condensation. Journal of Physical Chemistry 64:1184-1187. 1960.

39. Pierce, Conway and R. Nelson Smith. Adsorption in capillaries. Journal of Physical Chemistry 57:64-68. 1953.

40. Plachenov, T.G. The development of porosimeters for the study of the structure of porous bodies by method of mercury impregnation under pressure. Journal of Applied Chemistry. U.S.S.R. 28:223-229. 1955.

41. Schull, C.G. The determination of pore size distribution from gas adsorption data. Journal of the American Chemical Society 70:1405-1410. 1948.

42. Slabaugh, W.H. Adsorption characteristics of homoionic bentonites. Journal of Physical Chemistry 63:436-437. 1959.

43. Sverdrup, H.U., Martin W. Johnson and Richard H. Fleming. The Oceans. Englewood Cliffs, N.J., Prentice-Hall Inc., 1960. 1087p.

44. Warsham, Charlott E. and Rustum Roy. Classification and scheme for the identification of layer silicates. Geological Society of America Bulletin 72:1455-1492. 1961.

45. Weiser, Harry Boyer. A textbook of colloidal chemistry 2d.ed. New York, John Wiley and Sons Inc., 1958. 444p.

APPENDIXES

APPENDIX 1

Information extrapolated from desorption isotherms for computer calculations of pore size distribution

P/P_o	Weight adsorbed at each increment, mg/g Sample No. 60	No. 95	No. 118
1.000	40.1	21.0	11.3
.967	38.1	19.0	10.2
.953	37.3	18.2	9.9
.947	37.1	17.9	9.7
.937	36.6	17.5	9.5
.927	36.2	17.1	9.3
.915	35.6	16.6	9.1
.897	34.9	15.9	8.8
.870	33.7	15.1	8.5
.823	31.6	13.9	7.9
.788	30.0	13.3	7.6
.763	29.3	12.9	7.5
.733	28.7	12.6	7.4
.695	27.9	12.1	7.0
.675	27.5	11.8	6.9
.650	27.1	11.5	6.7
.625	26.8	11.1	6.5
.600	26.5	10.7	6.4

APPENDIX 1 Continued

P/P_o	Weight adsorbed at each increment, mg/g Sample No. 60	No. 95	No. 118
.580	26.1	10.4	6.3
.560	25.7	9.9	6.2
.540	25.2	9.5	6.0
.520	24.4	9.0	5.9
.500	23.5	8.8	5.8
.480	22.7	8.6	5.6
.460	21.3	8.4	5.5
.440	20.8	8.2	5.4
.420	20.4	8.0	5.2
.400	20.1	7.8	5.0
.380	20.0	7.6	4.9
.352	18.7	7.4	4.6

APPENDIX 2

Pore size distribution readout from ALWAC No. 3E computer

P/P_o	W, mg	$\sum A_p$, m^2/g	$\bar{r}_p$, Å	$\Delta v/\bar{r}_p$	L, m x 10^{-6}
1.000	45.00				
.967	41.40	1.072	500.0	.0681	3.4114
.953	40.30	1.155	258.4	.0121	.5091
.947	39.90	1.195	202.4	.0173	.3173
.937	39.30	1.268	175.8	.0218	.6613
.927	38.70	1.360	150.2	.0323	.9766
.915	38.00	1.492	129.9	.0446	1.6085
.897	37.20	1.668	110.0	.0473	2.5457
.870	35.90	2.061	89.6	.0872	6.9848
.823	34.10	2.805	69.1	.1241	17.1357
.788	32.80	3.524	53.9	.2023	21.2426
.763	32.00	4.027	46.5	.2268	17.2333
.733	31.10	4.678	41.4	.2718	25.0116
.695	30.00	5.618	36.4	.3475	41.0728
.675	29.70	5.809	32.9	.1453	9.2066
.650	29.00	6.551	30.6	.4806	38.5662
.625	28.40	7.207	28.4	.4514	36.8195
.600	27.50	8.454	26.4	.9031	75.0265
.580	26.90	9.284	24.9	.7849	53.1266
.560	26.10	10.576	23.6	1.2653	87.1292
.540	25.30	11.937	22.4	1.3763	96.5279
.520	24.50	13.368	21.4	1.4902	106.5972
.500	23.60	15.124	20.4	1.8778	137.1820
.480	22.60	17.232	19.4	2.3089	172.5158

APPENDIX 2 Continued

P/P_o	W, mg	$\sum A_p, m^2/g$	$\bar{r}_p$, Å	$\Delta v/\bar{r}_p$	L, m x 10^{-6}
.460	22.00	18.266	18.6	1.1563	88.4982
.440	21.70	18.423	17.8	.1798	14.1160
.420	21.40	18.616	17.0	.2226	17.9687
.400	21.10	18.842	16.3	.2654	22.0620
.380	20.80	19.101	15.6	.3076	26.3918
.352	20.50	19.027	14.9	-.0630	- 7.8831

APPENDIX 3

Flow Chart of Main Program

(x indicates x is fetched from the pre-tabulated value table; 0(x) is the old value of x, i.e., that from the last line. The pre-tabulating subprogram starts with 0(n) = 9 and arbitrarily fixes the second value of $\bar{r}_p$ as 500.)

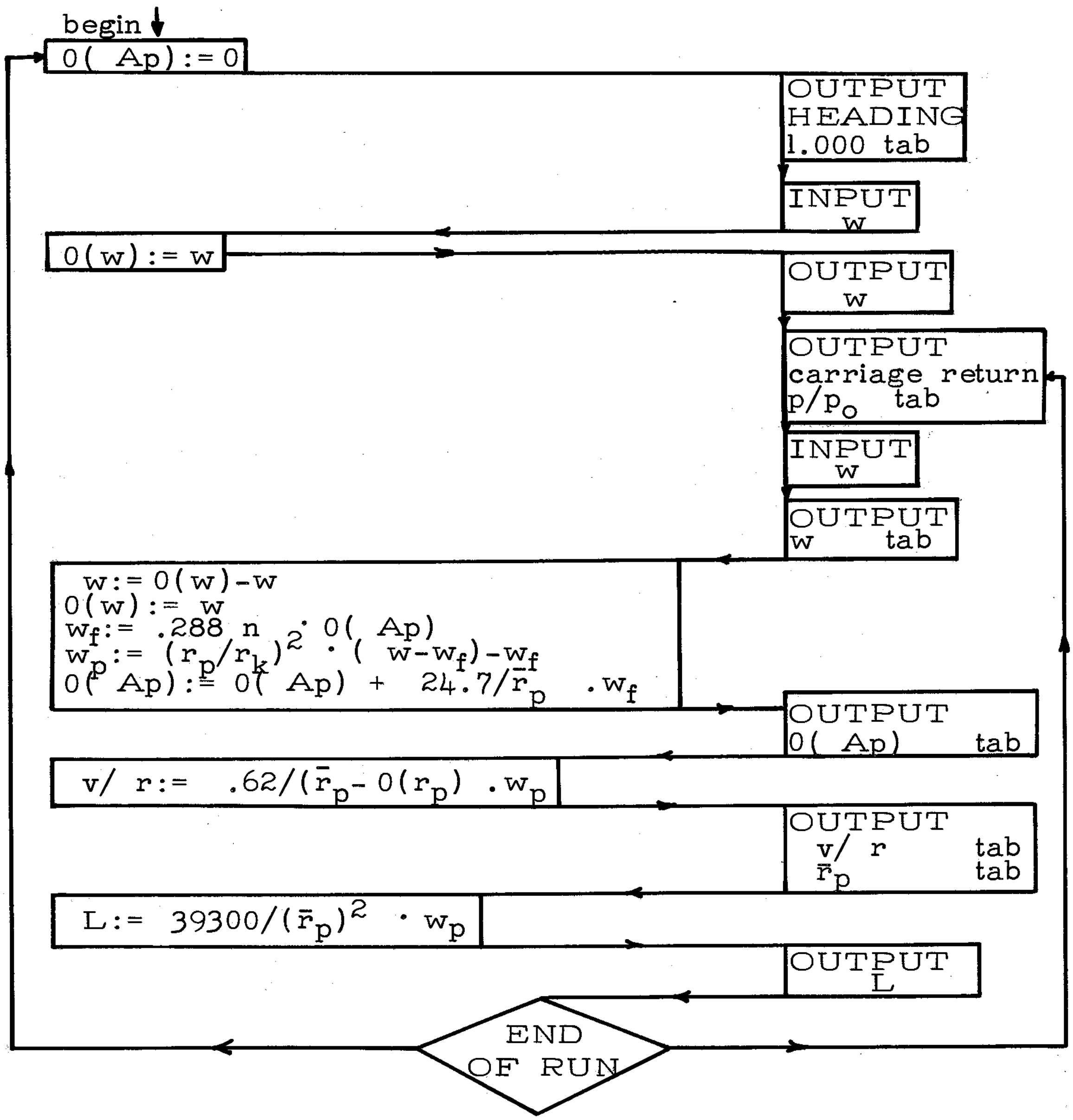

APPENDIX 4

PROGRAM USE

The data pre-tabulating routine, patchily in channels 5d, 5e (entry code 5e00 up to 5e88), assumes the first value of p/p_o is 1, accepts a fixed number of p/p_o values, then halts. Channel word 5d39 may be made 81601100 to jump directly into the main program.

Let Δ be the number of lines to be output, i.e., the number of p/p_o values including 1. Then we must have Δ in the address part of channel halfword 6001, Δ-1 in ad(5e88) and ad(5e8f), and 61+Δ in ad(5e92) and ad(6130), all in hexadecimal. At present Δ = 1e hexadecimal = 30 decimal. A table is generated using the first eight words of each of the Δ channels following channel 61.

The p/p_o data are of the form .xxx, x a random decimal digit, and are input as a floating point fraction followed by a repeat of the digits. Thus if .897 is a p/p_o value, the input form will be .897 897, with the usual liberties as to the form of the floating point input.

Entry code for the main program, in channels 60 and 61, is 6000. This program uses the table in channels 62 through 61+Δ base 16, controls format, calculates and outputs the body of results, and resets. Care should be taken that each set of data input has the correct number of w values, as the program counts inputs, but does not search for a run-terminating character. Aside from that the algorithm is remarkably stable. With Δ = 30, the main program punches each run output in about one minute fifty-five seconds.

A specified-format floating point output subroutine is in channel 5f and used in WS III. Caution: do not substitute a similar routine which uses the C register.

APPENDIX 4 Continued

Machine Coding

5e 1

00	0000	0000	80	01	612a	4900	81	02	872a	9de9	82	03	cb01	5b33	83
04	0000	0000	84	05	29e5	a707	85	06	5b3b	493b	86	07	4136	9de7	87
08	0000	951d	88	09	6100	4900	89	0a	4127	9de9	8a	0b	5b3b	9d61	8b
0c	8520	834d	8c	0d	29e5	a701	8d	0e	5b2b	9d40	8e	0f	cb07	161d	8f
10	872e	9d60	90	11	6100	4900	91	12	872a	c87f	92	13	1fbd	5b3b	93
14	493b	792a	94	15	413b	873c	95	16	5ba7	4136	96	17	9de9	5bac	97
18	f303	4900	98	19	9d60	493b	99	1a	4936	9d67	9a	1b	9de7	2e00	9b
1c	1115	0000	9c	1d	5bae	4123	9d	1e	5b2f	9de7	9e	1f	cb02	1720	9f

5d 2

20	5b87	4132	a0	21	9de9	cb04	a1	22	9d67	2e00	a2	23	-9885	f284	a3
24	c732	9d61	a4	25	413f	5bb2	a5	26	4932	1193	a6	27	-c04f	d882	a7
28	2400	5ba3	a8	29	9de7	413a	a9	2a	0000	007e	aa	2b	ba2e	8d7f	ab
2c	4137	493f	ac	2d	5bae	9de9	ad	2e	0000	000a	ae	2f	9374	bc7f	af
30	cb05	9de9	b0	31	cb06	7900	b1	32	fa00	008a	b2	33	e666	6682	b3
34	cb03	413f	b4	35	cb00	1710	b5	36	9000	0084	b6	37	c599	9a85	b7
38	5b32	9d67	b8	39	1b39	0000	b9	3a	9984	0090	ba	3b	0000	0000	bb
3c	5bad	413e	bc	3d	1b3d	5b32	bd	3e	9eb8	5280	be	3f	0000	0000	bf

5f 3

40	c349	a508	c0	41	2926	11d1	c1	42	0000	a702	c2	43	3200	d500	c3
44	3716	c143	c4	45	f1cd	97ac	c5	46	61d7	a701	c6	47	df5f	554c	c7
48	a710	3716	c8	49	0000	a701	c9	4a	5bab	17c2	ca	4b	114f	f541	cb
4c	2800	c14c	cc	4d	a701	61d0	cd	4e	330e	a100	ce	4f	17cb	1f47	cf
50	7fb1	6553	d0	51	a701	5ba4	d1	52	bd45	5543	d2	53	5749	9fa0	d3
54	4dce	c545	d4	55	17c9	ed58	d5	56	e957	11de	d6	57	d500	dd00	d7

APPENDIX 4 Continued

58	554c	330e	d8	59	4545	2926	d9	5a	e75b	1957	da	5b	0000	000a	db
5c	3e00	a101	dc	5d	5543	114a	dd	5e	df00	175a	de	5f	3302	114f	df

60 1

00	8361	855f	80	01	951e	490b	81	02	0300	0400	82	03	0200	0300	83
04	872e	9512	84	05	9d60	4906	85	06	0000	0000	86	07	0300	0100	87
08	7820	f705	88	09	793b	c962	89	0a	0000	0000	8a	0b	0000	0000	8b
0c	1708	1101	8c	0d	11a0	0000	8d	0e	5b6c	b8cb	8e	0f	6166	df00	8f
10	4485	9752	90	11	1055	12fc	91	12	0115	38d0	92	13	058a	164e	93
14	5d4b	d44a	94	15	7c05	255c	95	16	0367	546a	96	17	634f	544e	97
18	7c04	54e2	98	19	5015	3dd0	99	1a	0385	38d0	9a	1b	0f65	3d43	9b
1c	51f0	1152	9c	1d	7740	3852	9d	1e	6340	d682	9e	1f	7f86	1858	9f

61 2

20	7902	9d40	a0	21	4106	5bc9	a1	22	9d67	490a	a2	23	5ba4	410a	a3
24	df4d	17a8	a4	25	5f06	9d67	a5	26	b703	5ba6	a6	27	9de7	793f	a7
28	1104	872e	a8	29	490a	b701	a9	2a	9de7	5b0b	aa	2b	9d40	df4c	ab
2c	9d60	872a	ac	2d	5bae	410b	ad	2e	9d61	490b	ae	2f	b706	5ba9	af
30	c87f	b700	b0	31	9de7	5b0a	b1	32	7903	9d40	b2	33	410a	9de7	b3
34	f705	df4c	b4	35	490a	9d67	b5	36	df4c	4185	b6	37	1120	0000	b7
38	5db9	793b	b8	39	b702	5ba5	b9	3a	7907	9d40	ba	3b	0200	0200	bb
3c	9d40	df42	bc	3d	9de7	5b0a	bd	3e	df4c	b704	be	3f	0300	0400	bf

Tallies: 69dfc291, c3b946a1, 3cd8fe7f, 4263faca, and 272b6773 in order.

APPENDIX 5

Comparison of B.E.T. W_m values with W_m values obtained at $P/P_o = 0.2$ from W/n for marine sediments. $P/P_o = 0.2 = 15.2$ cm Hg.

No.	Sample No.	W, mg/g at $P/P_o = 0.2$	W/n n=1.25	B.E.T. W_m, mg/g	Deviation mg/g	0/0 Deviation
1	6107-6	23.2	18.5	17.9	-0.60	+3.4
2	3	8.90	7.14	7.3	+0.16	-2.2
3	6	21.5	17.2	16.7	-0.50	+3.0
4	6	23.0	18.4	17.5	-0.90	+5.1
5	6	23.0	18.4	17.9	-0.50	+2.8
6	93	9.00	7.2	7.3	+0.10	-1.4
7	6	21.7	17.3	16.9	-0.40	+2.3
8	6	21.8	17.4	16.7	-0.70	+4.2
9	110	26.0	20.8	20.0	-0.80	+4.0
10	93	9.50	7.60	7.30	-0.30	+4.1
11	26	6.90	5.52	5.55	+0.03	-0.5
12	14	9.70	7.76	7.10	-0.66	+9.3
13	42	9.80	7.85	7.64	-0.21	+2.7
14	93	10.2	8.17	8.12	-0.05	+0.6
15	110	28.1	22.4	21.7	-0.70	+3.2
16	26	7.20	5.76	5.92	+0.16	-2.7
17	93	10.1	8.05	7.82	-0.17	+2.2
18	6	19.6	15.6	14.7	-0.90	+6.1
19	95	9.60	7.70	7.70	0	0
20	93	9.00	7.20	7.15	-0.05	+0.7
21	42	10.2	8.17	8.07	-0.10	+1.2
22	14	9.90	7.94	7.70	-0.24	+3.3

APPENDIX 5 Continued

No.	Sample No.	W, mg/g at P/P_o=0.2	W/n n=1.25	B.E.T. W_m, mg/g	Deviation mg/g	0/0 Deviation
23	60	17.2	13.8	13.0	-0.80	+6.1
24	9	12.6	10.1	9.70	-0.40	+4.1
25	94	8.40	6.74	6.67	-0.07	+1.1
26	9	12.4	9.94	9.65	-0.29	+3.0
27	95	7.20	5.76	5.72	-0.04	+0.7
28	94	7.50	6.00	5.96	-0.04	+0.7
29	29	16.3	13.0	12.6	-0.40	+3.2
30	14	6.20	4.96	4.56	-0.40	+8.8
31	26	4.80	3.84	3.73	-0.11	+3.0
32	6	13.6	10.9	11.5	+0.60	-5.2
33	14	4.80	3.84	4.04	+0.20	-5.0
34	93	4.60	3.58	3.87	+0.31	-8.0
35	110	17.5	14.0	15.2	+1.20	-7.6
36	95	6.50	5.20	4.90	-0.30	+6.1
37	42	4.80	3.82	4.38	+0.36	-8.2
38	26	4.50	3.60	3.65	-0.05	+1.4
39	95	5.70	4.56	4.86	-0.30	+6.2
40	29	15.6	12.5	12.6	-0.10	+0.8
41	120	0.85	0.68	0.77	-0.09	+11.6
42	95	6.10	4.88	4.92	-0.04	+0.8
43	13	5.60	4.48	4.53	-0.05	+1.1
44	60	16.3	13.0	13.1	-0.10	+0.8
45	118	3.90	3.13	3.06	+0.07	-2.3